University of Stavanger

FACULTY OF SCIENCE AND TECHNOLOGY

MASTER'S THESIS

Study programme/specialisation: Engineering Structures and Materials / Civil Engineering Structures	Spring semester, 2021 Open
Author: Isabel Mercedes La Torraca Lopez	
Programme coordinator: Sudath Siriwardane Supervisor(s): Fredrik Bjørheim	
Title of master's thesis: Material characteristics of 3-D printed steel	
Credits: 30	
Keywords: Additive manufacturing AM processes Fatigue Mechanical properties 17-4 PH SS	Number of pages: 73 Stavanger, 10.07.2021

ABSTRACT

Additive manufacturing of metals is a technology where metal parts are built layer by layer from a 3D model. To do this a heat source is used to melt metal powder or metal rods. There is a large selection of processes that uses different materials and layer deposition techniques. As metal additive manufacturing is a growing field, it is important to understand the different processes and the properties of the metal additive manufactured components. This thesis provides an overview of the most common steel AM processes, process parameters, advantages and disadvantages of the processes and post process treatments, along with the processing challenges with void formation, gas porosity, lack of fusion, residual stresses, cracks and microstructural heterogeneity of the metal additive manufactured parts. Special attention is paid to the fatigue performance of the metal AM parts. To accomplish this, a review of previous research was undertaken. The mechanical properties of as-sintered 17-4 PH stainless steel specimens manufactured by a bound metal deposition process are also studied, and a brief evaluation with the optical light microscope is performed. Mechanical properties of the specimens such as yield strength, ultimate strength, ductility, and modulus of elasticity are obtained by performing tensile tests. Tensile test results from this study show that the building orientation of the specimens relative to the applied loading direction as well as the support structures affects the tensile behavior of the material. Un-melted regions were observed with the optical light microscope.

PREFACE

This thesis is the final work to complete the master's degree in Civil Engineering Structures and Materials at the Department of Mechanical and Structural Engineering and Materials Science at the University of Stavanger, Norway. This work was performed during the spring semester of 2021.

Throughout the writing of this thesis, I have received a great deal of support and assistance.

I would like to give thanks to my supervisor Fredrik Bjørheim, for his support, valuable guidance, and unlimited assistance throughout the whole writing process.

I would also like to give thanks to Jørgen Grøndsund and Jan-Tore Jakobsen for all the help with the production of the additive manufactured specimens and the experimental work, and to Johan A. Thorkaas and Mats Ingdal for the guidance and support with the specimen's preparation.

My appreciation and thanks to my husband and kids, you are always there for me. Special thanks to my son Rafael D. Rosales, for his endless patience support and motivation I could have not completed this thesis without your support. And finally, I want to give big thanks to my mother for her motivation all the way to this master's degree.

Stavanger, July 2021

Isabel La Torraca

TABLE OF CONTENT

ABSTRACT **2**

PREFACE **3**

LIST OF FIGURES **6**

LIST OF TABLES **8**

LIST OF ABREVIATIONS **9**

1. INTRODUCTION **12**

2. LITERATURE REVIEW **15**

2.1. Additive manufacturing of metals 15

2.2. AM of metal advantages over traditional manufacturing techniques 16

2.3. Additive manufacturing of metals processes 17

2.3.1. Powder bed fusion (PBF) processes 19

2.3.1.1. Powder bed fusion laser beam (PBF-L): 19

2.3.1.2. Powder bed fusion electron beam (PBF-EB): 20

2.3.1.3. Advantages of PBF systems: 20

2.3.1.4. Disadvantages of PBF systems: 21

2.3.2. Direct Energy Deposition (DED) processes 21

2.3.2.1. Direct energy deposition laser beam (DED-L): 22

2.3.2.2. Direct energy deposition electron beam (DED-EB): 22

2.3.2.3. Direct energy deposition plasma arc (DED-PA): 23

2.3.2.4. Advantages of DED systems: 24

2.3.2.5. Disadvantages of DED systems: 24

2.3.3. Bound metal deposition (BMD) and other metal AM technologies 24

2.4. Process parameters 26

2.5. Most common defects found in additive manufactured metals 27

2.5.1. Gas porosity 28

2.5.2. Lack of fusion (LOF) voids 29

2.5.3. Loss of alloying elements 29

2.5.4. Cracks 29

2.5.5. Microstructural heterogeneity 30

2.6. Residual stress in additive manufactured metal parts 30

2.7. Fatigue in additive manufactured metals 31
2.8. Post AM fabrication Processes 38
2.9. Composition of AM 17-4 PH Stainless Steel 39
2.10. Material tests 40
2.10.1. Tensile test 40
2.10.2. Optical Light Microscopic technique 44
3. EXPERIMENTAL DETAILS 45
3.1. Description of the AM technology used to manufacture the samples 46
3.2. Sample manufacturing 46
3.3. Sample preparation for OLM 50
3.4. Tensile test 52
3.5. Optical Light Microscopy (OLM) evaluation 52
4. RESULTS 53
4.1. Tensile test results 53
4.2. Optical Light Microscope results 58
5. DISCUSSION 61
5.1. Literature review: 61
5.2. Tensile test: 62
6. CONCLUSION 63
7. REFERENCES 65
FIGURES 70
TABLES 72

LIST OF FIGURES

Figure 1: PBF-L system (DebRoy et al., 2018). 19
Figure 2: PBF-EB system (Gibson et al., 2015). 20
Figure 3: DED-L system with metal powder used as feedstock material (DebRoy et al., 2018). 22
Figure 4: DED-EB system with metal wire used as feedstock material (DebRoy et al., 2018). 23
Figure 5: DED-PA system with metal wire used as feedstock material (DebRoy et al., 2018). 23
Figure 6: BMD 3D Printer. 25
Figure 7: BMD Debinder. 26
Figure 8: BMD Sinter. 26
Figure 9: Defects in PBF-L Ti-6Al-4V alloy (A) porosity (entrapped gas) and lack of fusion voids, (B) cracking from a porosity (entrapped gas), (C) lack of fusion voids, (D) crack initiation and growth from lack of fusion voids defects (Ali Fatemi et al., 2019). © 2019 Wiley Publishing Ltd. 28
Figure 10: Building direction. 34
Figure 11: Built orientation with respect to the defect formed during fabrication 37
Figure 12: Engineering strain-stress curve (Davis, 2004, p. 14). 42
Figure 13: Standard tensile bar with dimension according to ASTM E8/E8M. 46
Figure 14: BMD tensile testing sample manufactured at the XY-flat building orientation. ... 47
Figure 15: BMD tensile testing sample manufactured at the XY-sided building orientation. 48
Figure 16: BMD tensile testing sample manufactured at the ZX building orientation. 48
Figure 17: Illustration of the 2 building directions V and H. 49
Figure 18: Raster strategy for an XY-flat subsize tensile specimen. 49
Figure 19: Specimen mounted in transparent resin. 51
Figure 20: fracture location of all tensile specimens. 53
Figure 21: Yield strength for all the test specimen and for the reference value. 54
Figure 22: Ultimate tensile strength for all the test specimen and for the reference value. 55
Figure 23: Young´s modulus for all the test specimen and for the reference value. 55
Figure 24: Elongation at break for all the test specimen and for the reference value. 56

Figure 25*: Engineering stress-strain curve of AM 17-4 PH stainless steel in different building orientations.* 57
Figure 26: Top view of vertically printed specimens 58
Figure 27: Side view of vertically printed specimens. 59
Figure 28: Top view of horizontally printed specimens. 59
Figure 29: Side view of horizontally printed specimens 60

LIST OF TABLES

Table 1: Most customary types of metals alloys offered and its applications (Milewski, 2017, p. 187) 16
Table 2: AM metal machine manufacturers and their specific process names (Milewski, 2017, p. 133). 18
Table 3: Summary of the AM processes. 18
Table 4: Critical parameters that control DED and PBF processes (Dutta et al., 2019, p. 29). 27
Table 5: List of SLM steels present in the fatigue studies (Afkhami et al., 2019). 35
Table 6: Failure mechanisms of the PBF-L AM 17-4 PH Stainless Steel, PBF-L AM Ti-6Al-4V and wrought specimens under different conditions (Reza Molaei & Fatemi, 2019). 36
Table 7: Composition of AM 17-4 PH Stainless Steel. Adapted from *(Markforged, 2021).* ... 40
Table 8: Typical mechanical properties of Markforged 17-4 PH Stainless Steel samples as-sintered fabricated by the BMD method (Markforged, 2021). 40
Table 9: Tensile test results for all specimens (Markforged as-sintered represents reference values). 54

LIST OF ABREVIATIONS

3D	3 Dimensional
AM	Additive Manufacturing
ASTM	American Society for Testing and Materials
BMD	Bound Metal Deposition
CAD	Computer Aided Design
CNC	Computerized Numerical Control
DED	Direct Energy Deposition
DED-EB	Direct Energy Deposition Electron Beam
DED-GMA	Direct Energy Deposition Gas Metal Arc
DED-L	Direct Energy Deposition Laser
DED-PA	Direct Energy Deposition Plasma Arc
DMD	Direct Metal Deposition
DMP	Direct Metal Printing
DMLS	Direct Metal Laser Sintering
E	Young's modulus
EB	Electron Beam
EBAM	Electron Beam Additive Manufacturing
EBF3	Electron Beam Free Form Fabrication
EMB	Electron Beam Melting
GMA	Gas Metal Arc

HAZ	Heat Affected Zone
HCF	High Cycle Fatigue
HIP	Hot Isostatic Pressing
HT	Heat Treatment
ISO	International Organization for Standardization
L	Laser
LBM	Laser Beam Melting
LCF	Low Cycle Fatigue
LENS	Laser Engineered Net Shape
LMD	Laser Metal Deposition
LMF	Laser Metal Fusion
LOF	Lack of Fusion
OM	Optical Microscope
OLM	Optical Light Microscopy
PA	Plasma Arc
PA-DED	Plasma Arc Direct Energy Deposition
PBF	Powder Bed Fusion
PBF-EB	Powder Bed Fusion Electron Beam
PBF-L	Powder Bed Fusion Laser
PH	Precipitation Hardening
SLM	Selective Laser Melting

SLS	Selective Laser Sintering
SS	Stainless Steel
STL	Stereo-lithography
UTS	Ultimate Tensile Strength
YS	Yield Strength
YTS	Yield Tensile Strength

1. INTRODUCTION

Additive manufacturing (AM), often called 3D printing (Dass & Moridi, 2019; Frazier, 2014), can be defined as the process that fabricates complex or customized solid free form parts using computer aided design. The process consist of progressively adding layer by layer of materials, as opposed to conventional subtractive manufacturing technique that carves or shape a solid piece of material into the desired product (ASTM International, 2021a).

Additive manufacturing (AM) is changing the way products are designed and manufactured (Wang et al., 2019), and it has been extensively used in many industries (Ngo, Kashani, Imbalzano, Nguyen, & Hui, 2018) including the automotive, aerospace, energy, oil and gas, health care, industrial, and remanufacture industries, among others (Milewski, 2017, p. 8). The rapid growth in sales of commercial AM systems has proved that the technology has now gotten a critical acceptance level (DebRoy et al., 2018).

Metal AM is a growing sector of manufacturing that has captured much attention lately because of the large corporate investments in research centers, and multi-million-dollar government funding in advanced manufacturing programs (Milewski, 2017, p. 270). The press and technical journals are reporting constantly on the technology (Brandt, 2016). Equinor, the Norwegian national oil and gas company, has shown interest in producing the spare parts on the go for its offshore facilities, and AM is a possible way to do so.

Among the advantages of additive manufacturing technology, we can mention the design freedom, the possibility of fabricating complicated geometries with complex internal structures which are difficult to build using traditional manufacturing techniques (Zadi-Maad, Rohib, & Irawan, 2018); mass customization, to produce a number of customized parts, can be as cost-effective as to produce the same number of identical parts (Ngo et al., 2018); fast prototyping, the parts can be produced directly from the design, reducing the need of many conventional processing steps and expensive tooling (DebRoy et al., 2018); along with higher material efficiency (waste minimization) (Reza Molaei & Fatemi, 2019). Additionally, parts can be fabricated on site when required, decreasing or avoiding the inventory of spare parts (DebRoy et al., 2018).

Despite all the advantages of the additive manufacturing techniques, these can still face limitations like the control of the properties of its final product (Afkhami, Dabiri, Alavi, Björk,

& Salminen, 2019). Fabrication defects like pores, surface defects and voids, have been shown to notably influence AM materials. Furthermore, AM components have shown some metallurgical differences with conventional manufactured components (DebRoy et al., 2018).

There is a large selection of metal AM technologies which often include melting powder or wire feedstock, using laser or electron beam (Herzog, Seyda, Wycisk, & Emmelmann, 2016; Nezhadfar et al., 2019; Pegues et al., 2020). Among the most accepted AM technologies we can mention powder bed fusion (PBF), followed by direct energy deposition (DED) and bound metal deposition (BMD) (Dutta, Babu, & Jared, 2019, p. 311). The final AM part may be substantially different depending on the process used and the material, so it is important to understand the different processes to choose the right process base on the design requirements and the use of the final part (Milewski, 2017, p. 132).

The design of AM parts carrying critical loads is still at an early phase (Reza Molaei & Fatemi, 2019). Continuing research is desirable to properly understand the processes, properties and performances to produce reliable AM parts to gain more industry acceptance (Shamsaei, Yadollahi, Bian, & Thompson, 2015).

Previous investigations related to additive manufacturing of metals were reviewed and evaluated by comparing the results found. Special attention was given to the definition of additive manufacturing of metals, and to the processes and advantages over traditional manufacturing techniques. Investigations about what has been done in regard to fatigue of 3-D printed steel components was also performed as well as experimental work in regard to monotonic loading of AM 17-4 PH stainless steel specimens. The bound metal deposition (BMD) process was used to manufacture the specimens used for the experimental work. An optical light microscope was used for macrostructural evaluation of the AM 17-4 PH stainless steel specimens. The aim of this investigation is to briefly summarize the actual knowledge in this field and to complete the investigation with an experimental work willing to extend the knowledge of the AM 17-4 PH stainless steel.

Steel has been extensively used in different applications, and especially stainless steels are gaining more attention because of their outstanding oxidation and corrosion resistance (Zadi-Maad et al., 2018).

Since additive manufactured metals are used in many industries such as biomedical, aerospace, automotive, marine and offshore industry (Pegues et al., 2020), it is important to continue the

research to understand the relation between the microstructure, the processes, and the properties of the different AM steel components in order to be able to extends its use (Frazier, 2014).

2. LITERATURE REVIEW

This literature review summarizes the revision of previous investigations related to additive manufacturing of metals. This was performed by evaluating and comparing the results found in the previous investigations. It also includes the theory behind additive manufacturing of metals and additive manufacturing of metals methods. Additionally, the theory behind the experimental testing is presented.

2.1. Additive manufacturing of metals

Additive manufacturing of metals are processes that "consolidate feedstock materials […] into a dense metallic part by melting and solidification with the aid of an energy source" (DebRoy et al., 2018, p. 116).

The whole manufacturing process starts with a computer-modeled part that is sliced into multiple layers and is then developed in the AM printer, through iteratively building layer by layer in 3D space. Since the final geometry depends on the addition of each layer, it is called an additive process, contrary to the subtractive manufacturing processes (Dutta et al., 2019, p. 2). The metals usually printed using AM techniques are aluminum alloys, titanium alloys (Carneiro, Jalalahmadi, Ashtekar, & Jiang, 2019; Herzog et al., 2016; Milewski, 2017, p. 186), steel and nickel alloys (Herzog et al., 2016; Milewski, 2017, p. 186).

Among the applications of additive manufacturing of metals, we can mention:

- Aerospace industry.
- Automotive industry.
- Oils and gas industry.
- Energy industry.
- Engineered structures and materials.
- Medical and dental.
- General industrial markets.
- Remanufacture and repair.
- Tool and die.
- Artistic (Milewski, 2017, pp. 7-32).

The term AM represents various technologies. The level to which the desired material properties can be reached, repeated, or improved for a specific application will be affected by the right selection of AM materials and processes (Milewski, 2017, p. 55).

Table 1 below shows a list of the most customary types of metal alloys provided by the equipment vendor and the industry where they are used (Milewski, 2017, p. 187).

Table 1: Most customary types of metals alloys offered and its applications (Milewski, 2017, p. 187) .

Applications for the Common Additive Manufacturing Metals							
Alloy Type	**Aluminum**	**Maraging Steel**	**Stainless Steel**	**Titanium**	**Cobalt Chrome**	**Nickel Super Alloys**	**Precious Metals**
Aerospace	X		X	X	X	X	
Medical			X	X	X		X
Energy, Oil, Gas			X				
Automotive	X		X	X			
Marine Environment			X	X		X	
Machinability Weldability	X		X	X		X	
Corrosion Resistance			X	X	X	X	
High Temperature				X		X	
Tools and Molds		X	X				
Consumer Products	X		X				X

2.2. AM of metal advantages over traditional manufacturing techniques

Additive Manufacturing's (AM) advantages over the traditional manufacturing techniques include the production of complex or customized parts which are difficult to build using the

conventional processing methods and greater degree of design freedom without any tools or dies as compared to traditional manufacturing processes (DebRoy et al., 2018, p. 115). These parts can be made in one step which reduces the production cost by eliminating the assembly issue and the need for machining. Also, since AM builds near net shape parts, there is less, or no material waste compared to the traditional manufacturing techniques. Existing used and/or damaged parts can be repaired and/or remanufactured (Dutta et al., 2019, p. 323).

We can also name the ability of on-site fabrication of the replacement parts and the productions of parts on demands as some of the advantages of AM techniques (A. Fatemi, Molaei, & Phan, 2020; Ngo et al., 2018). The production of parts on demand reduces the inventory of spare parts (no large part warehouse inventories needed) and decreases the production time of a new part or a replacement part (DebRoy et al., 2018).

For all these reasons AM is now extensively accepted for the design and production of components in various industries including energy, medical, aerospace, and automobile (DebRoy et al., 2018, p. 116). However, despite the recent progress in the AM of metal technologies, there are some metallurgical differences between AM and conventional components such as anisotropic mechanical properties, residual stress, and defects unique to AM processes that need to be investigated (Wang et al., 2019).

For some applications, AM is not considered as a replacement for the conventional manufacturing processes. AM is considered as an additional tool that provides design freedom and reduces the time from design to market (Dutta et al., 2019, p. 7).

2.3. Additive manufacturing of metals processes

The additive manufacturing processes received different names and most of those names are assigned by the machine manufacturers, but the basis of the process is the same, to create a model from a 3D CAD program on a computer and then built the model up by adding layer by layer of materials using a heat source such as laser or electron beam. Some systems use metal powder as feedstock and other systems use metal wire (Herzog et al., 2016). In Table 2 (Milewski, 2017, p. 133), some manufacturers and their specific process names are listed.

Table 2: AM metal machine manufacturers and their specific process names (Milewski, 2017, p. 133).

Process	Process name	Manufacturer	ASTM category
DMLS	Direct Metal Laser Sintering	EOS	PBF-L
SLM	Selective Laser Melting	SLM Solutions	PBF-L
DMP	Direct Metal Printing	3D Systems	PBF-L
LaserCUSING®	LaserCusing	Concept Laser	PBF-L
EBM®	Electron Beam Melting	Arcam AB	PBF-EB
EBAM™	Electron Beam Additive Manufacturing	Sciaky Inc.	DED-EB
LENS®	LENS	Optomec	DED-L
DMD®	Direct Metal Deposition	DM3D Technology LLC	DED-L

It is important to understand the basic system configurations of the different additive manufacturing processes to properly choose the right process according to the needs, since they all present different characteristics and capabilities as well as different advantages and limitations (Milewski, 2017, p. 131).

The ASTM Standard F2792 defines the AM processes into two categories, Direct Energy Deposition (DED) and Powder Bed Fusion (PBF). Additional classifications depend on the heat source used, including laser-based (L), electron-beam-based (EB), plasma-arc-based (PA), and gas-metal-arc-based (GMA). The material for the AM processes can be supplied by powder or wire feed (DebRoy et al., 2018, pp. 116, 117).

Table 3 shows a summary of the AM technologies:

Table 3: Summary of the AM processes.

PROCESS	Direct Energy Deposition (DED)			Power Bed Fusion (PBF)	
Feedstock	Powder	Wire	Wire	Powder	
Heat source	Laser L	E-Beam EB	Electric arc	Laser	E-Beam
Nomenclature	DED-L	DED-EB	DED-PA	PBF-L	PBF-EB

2.3.1. Powder bed fusion (PBF) processes

In powder bed fusion (PBF) processes, the metal powder is spread by a recoating blade or roller in thin layers and melted via laser or electron beam over the previous layer to build up a 3D-part (DebRoy et al., 2018, p. 118). PBF processes are limited to small scale products but give parts with very good mechanical properties and smooth surface (Zadi-Maad et al., 2018).

Different steel materials have been processed successfully using PBF technology, including 316L / 304 /15-5P / 17-4 PH Stainless Steel, Ti alloys, Ni alloys, Cu alloys, Al alloys and Co alloys (Dutta et al., 2019, p. 23).

2.3.1.1. Powder bed fusion laser beam (PBF-L):

PBF-L is the most applied technology. PBF-L is the powder bed process that uses a laser beam as heat source to melt and fuse the metal powder as shown in Figure 1 (DebRoy et al., 2018). Downward facing structures and overhangs can be built, but supplementary support structures need to be added to the design. It is limited to build volume sizes of around 400 mm x 400 mm x 800 mm. Deposit surface quality is the best of all present metal AM systems (Milewski, 2017, pp. 37,38). PBF-L technologies are also referred to as direct metal laser sintering (DMLS), selective laser melting (SLM), selective laser sintering (SLS), or direct metal printing (DMP) (Milewski, 2017, p. 133), as shown in Table 1 (page 16). Additionally, they may be referred to as laser beam melting (LBM), laser CUSING, laser metal fusion (LMF), among other names (Herzog et al., 2016).

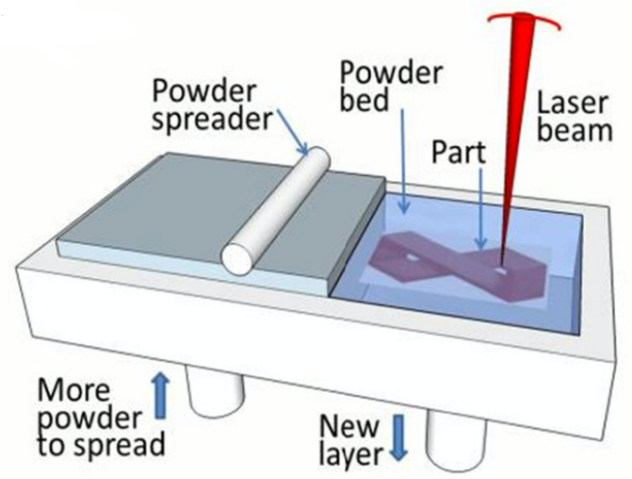

Figure 1: PBF-L system (DebRoy et al., 2018).

2.3.1.2. Powder bed fusion electron beam (PBF-EB):

PBF-EB, also referred to as electron beam melting (EBM) (Milewski, 2017, p. 133), is the powder bed process that uses an electron beam as heat source to melt and fuse the metal powder as shown in Figure 2 (Gibson, Rosen, & Stucker, 2015). This method is limited to build volume sizes of around 350 mm x 350 mm x 380 mm. Compared to PBF-L, it produces rougher surface finish. The design and use of support structures to build overhangs is reduced using PBF-EB methods (Milewski, 2017, p. 39).

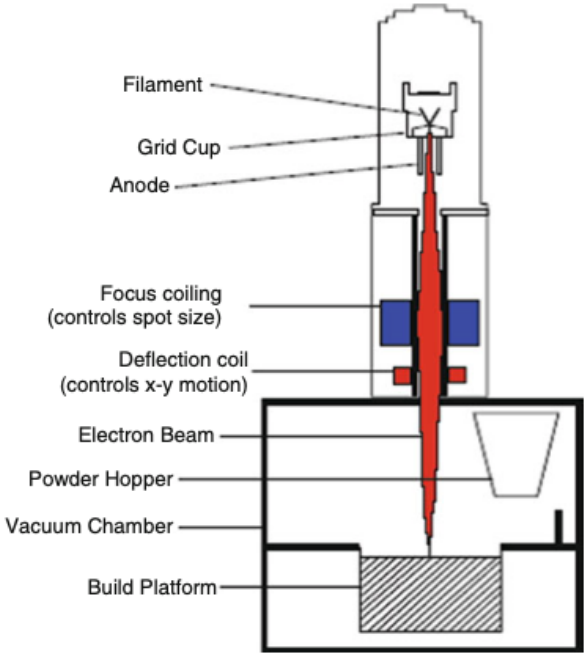

Figure 2: PBF-EB system (Gibson et al., 2015).

2.3.1.3. Advantages of PBF systems:

- Broad selection of CAD software to generate STL files as well as editing software that help on the preparation for 3D printing.
- Multiple replicas of the same part may be built in one build cycle as well as multiple replicas of different parts.
- Rapid prototype time to market.
- Overhangs and closed cooling passages are possible to fabricate.
- Good precision parts (Milewski, 2017, pp. 135-139).

- Complex structure with fine details.
- Better surface finish (A. Fatemi et al., 2020).

2.3.1.4. Disadvantages of PBF systems:

- Limited to small size parts.
- Slow deposition rate.
- A substantial volume of powder is required for the process that does not become part of the final product, generating the necessity of more reuse or recycling of material and its associated cost.
- Handling and storage of powdered metals can be difficult, therefore engineering and administrative controls for the safe use of powders is required.
- Parts have residual stress often requiring post-processing to get the wanted properties.
- High cost and limited supply of appropriate powder material (Milewski, 2017, pp. 140-147).
- Residual stress can cause distortion.
- Limited for repairing and for adding metal on existing parts.
- Difficult and not commercially available the use of multiple materials on single build (Dutta et al., 2019, pp. 23, 55-73).

2.3.2. Direct Energy Deposition (DED) processes

In DED processes, the metal powder or metal wire is introduced to a heat source, laser, electron beam or plasma arc which melts the material as it is being deposited layer by layer in a melt pool to build up a 3D-part (DebRoy et al., 2018). The AM DED processes can be used not only to create new parts but also to coat existing parts (Halada & Clayton, 2018).

Different steel materials have been processed successfully using DED technology, including 316L / 304 / 15-5P / 17-4 PH Stainless Steel, Ti alloys, Cu alloys, Al alloys, among others (Dutta et al., 2019, p. 21).

2.3.2.1. Direct energy deposition laser beam (DED-L):

DED-L is the process that uses a laser beam as a heat source to melt the metal powder or metal wire into the molten pool as shown in Figure 3 (DebRoy et al., 2018). The build volume size is of around 1500 mm x 900 mm x 900 mm (Milewski, 2017, pp. 39-41). DED processes that use laser beams (DED-L) are usually referred to as laser engineer net shape (LENS), direct metal deposition (DMD), and laser metal deposition (LMD) (Milewski, 2017, p. 133). Additionally, they may be referred to as laser cladding or laser deposition welding (Herzog et al., 2016). Laser directed energy deposition (DED-L) methods share many advantages and disadvantages with laser powder bed fusion (PBF-L) methods, but they also have remarkable differences.

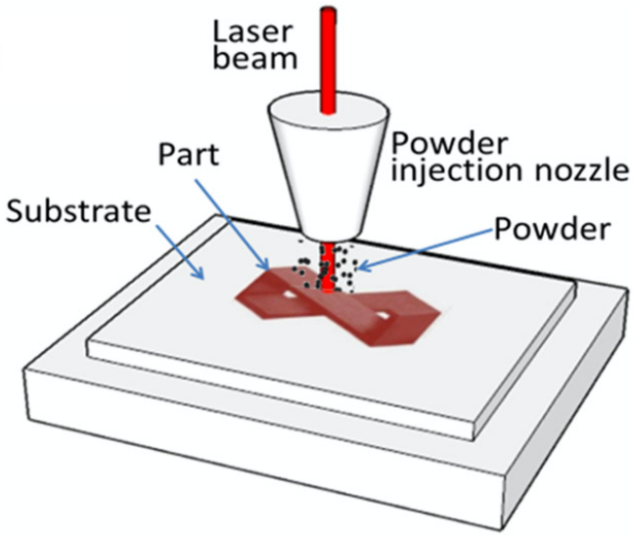

Figure 3: DED-L system with metal powder used as feedstock material (DebRoy et al., 2018).

2.3.2.2. Direct energy deposition electron beam (DED-EB):

DED-EB is the process that uses an electron beam as a heat source to melt the metal powder or metal wire into the molten pool as shown in Figure 4 (DebRoy et al., 2018). The build volume size is of around 1854 mm x 1194 mm x 826 mm, being this one advantage of the technology (Milewski, 2017, p. 42). DED processes that use an electron beam (DED-EB) are usually referred to as electron beam freeform fabrication (EBF3) and electron beam additive manufacturing (EBAM).

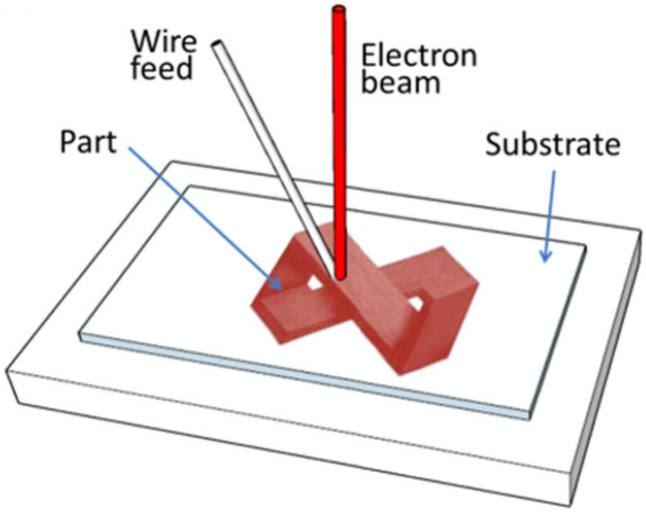

Figure 4: DED-EB system with metal wire used as feedstock material (DebRoy et al., 2018).

2.3.2.3. Direct energy deposition plasma arc (DED-PA):

DED-PA is the process that uses an electric arc as a heat source to melt the metal wire similar to fusion welding as shown in Figure 5 (DebRoy et al., 2018). It does not match the precision of PBF-L or PBF-EB but provides near-net-shape metal objects at a much lower cost. Commonly used for repairing or adding material to existing components. Additional machining and finishing are required as well as post-processing to get the desired properties. The build volume size is similar to DED-EB processes. DED processes that use plasma arc are also referred to as (PA-DED) (Milewski, 2017, pp. 42, 43, 133, 166).

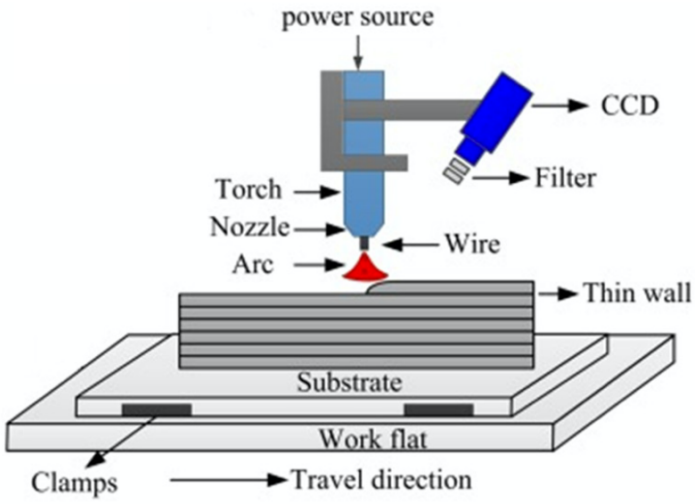

Figure 5: DED-PA system with metal wire used as feedstock material (DebRoy et al., 2018).

2.3.2.4. Advantages of DED systems:

- The use of multiple materials during the building process.
- Repair of existing parts.
- More variety of metal powder alloy available.
- Higher building rates compared to PBF (Milewski, 2017, pp. 39, 40, 151-155).
- Faster fabrication process.
- Building of larger parts (A. Fatemi et al., 2020).
- Metal addition on existing parts.
- Lower cost of the powder since the particle size and shape required for DED processes is less strict than for PBF processes.
- Some of the safety concerns with powder are decreased with the use of wire feedstock (Dutta et al., 2019, pp. 21, 55-73).

2.3.2.5. Disadvantages of DED systems:

- Less complex shapes because of complex path planning.
- The support structure needed to begin the buildup of the part may be harder to remove in comparison to PBF-L support (Milewski, 2017, pp. 155-157).
- Large overhangs and closed cooling passages are not possible to build.
- Parts have residual stress often requiring post-processing like HT and HIP to get the wanted properties.
- Residual stress can cause distortion.
- Limited material available for wire feeding systems (Dutta et al., 2019, pp. 22, 55-73).
- Rough surfaces compared to PBF processed parts requiring additional machining and finishing (Zadi-Maad et al., 2018).

2.3.3. Bound metal deposition (BMD) and other metal AM technologies

There are other additive manufacturing technologies, like the Binder Jet Technology, Cold Spray Forming and Bound Metal Deposition (BMD) that start with a computer model and build up a metal part. These technologies are not very popular yet (Dutta et al., 2019, p. 24).

The Bound Metal Deposition (BMD) technology, being commercialized by Desktop Metal, is an extrusion-based metal AM process where rods of bound metal are heated and extruded onto the build tray to form a metal part. In this technology, the feedstock material (bound metal rods) are a mixture of metal powder and plastic binder. After the part is printed, most of the plastic binder is dissolved and removed using a debind process. The debind process consists of placing the part in a debinding fluid in the debinder for several hours. After this, the part is sintered to bond the metal particles together and form a full metal part. The sintering takes place in a furnace with a slow uniform heat, generating minimal stresses. One of the advantages of this technology is that no residual stresses are generated since the use of a heat source is not part of the printing process. Removing the support structure is very easy. One disadvantage is that the process does not print full-density parts, that is why the sintering post process is required to improve strength. Markforged is one of the companies that has been using this extrusion technology to print metals (Dutta et al., 2019, pp. 7, 25). The printer, the debinder and the furnace can be seen in Figure 6, Figure 7, and Figure 8 respectively.

Figure 6: BMD 3D Printer.

Figure 7: BMD Debinder.

Figure 8: BMD Sinter.

2.4. Process parameters

The processes of AM have many parameters involved that besides affecting the process also affect the final properties and microstructure of the AM parts, so it is important to know and control these process parameters. These process parameters can include laser power, scanning speed, layer thickness, build direction, powder flow rate, among others (Zadi-Maad et al., 2018).

In particular PBF and DED processes have a large number of process parameters, and this might be one of the challenges when using these manufacturing technologies. Table 4 (Dutta et al., 2019, p. 29) shows these parameters.

Table 4: Critical parameters that control DED and PBF processes (Dutta et al., 2019, p. 29).

	DED	PBF
Heat source	Type (electron beam, laser wavelength, or gas-metal arc)	Type (electron beam or laser)
	Heat source power (W)	Heat source power (W)
	Spot or beam size (mm)	Spot or beam size (μm)
Feedstock	Type—powder or wire	Type—powder
	Powder size (μm), particle size distribution, and morphology or wire size (μm)	Powder size (μm), particle size distribution, and morphology
	Powder feed rate (g/min) or wire feed rate (m/min)	Powder layer thickness (μm)
	Preheat (applied to only wire) (ϱC)	Preheat applied to powder bed for some applications
Machine parameters	Traverse speed (mm/min)	Scan speed (m/s)
	Nozzle gases—gas type and flow rates (L/min)	Powder cover gas flow rate (L/min)
	Chamber environment—inert gas chamber for reactive metals, vacuum for electron beam processing, temperature, O_2 level, humidity level	Chamber environment—inert gas chamber for reactive metals, vacuum for electron beam processing, temperature, O_2 level, humidity level
Design and programing parameters	Deposition layer thickness (μm)	Fused layer thickness (μm)
	Spacing between successive tracks—step over (mm)	Spacing between successive tracks—hatch spacing (μm)
	Toolpath strategy	Toolpath strategy

2.5. Most common defects found in additive manufactured metals

The processes of AM have many parameters involved that besides affecting the process also affect the final product. An unsuitable selection of process parameters can lead to defects like loss of alloying elements, porosity, lack of fusion voids, delamination as a result of the lack of fusion voids, and cracks (Dutta et al., 2019, pp. 31-39). Understanding these defects and the

way they are affected by the process parameters is important to obtain good quality components (Milewski, 2017, p. 31). Examples of some of these defects are shown Figure 9 (Ali Fatemi et al., 2019).

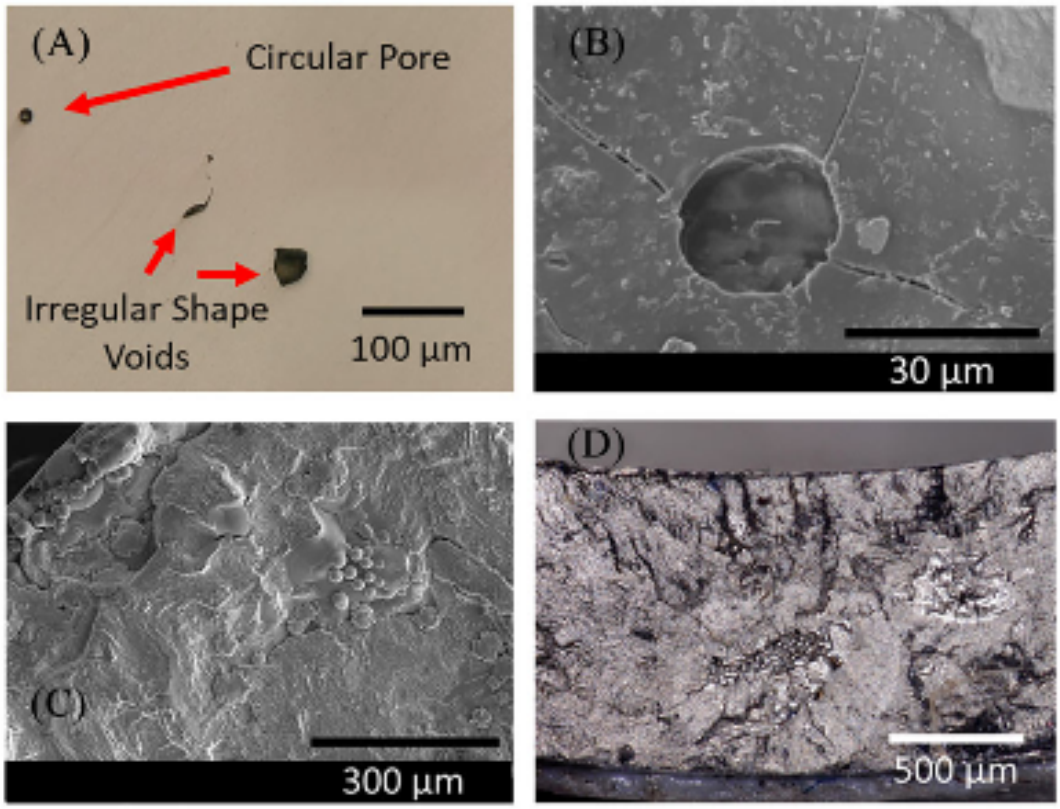

Figure 9: Defects in PBF-L Ti-6Al-4V alloy (A) porosity (entrapped gas) and lack of fusion voids, (B) cracking from a porosity (entrapped gas), (C) lack of fusion voids, (D) crack initiation and growth from lack of fusion voids defects (Ali Fatemi et al., 2019). © 2019 Wiley Publishing Ltd.

2.5.1. Gas porosity

Gas porosity is a common defect in metal AM parts linked to adverse effects on its mechanical properties and performance (DebRoy et al., 2018, p. 135). Gas porosity is often spherical in shape. Its formation is assumed to be the result of gas entrapped inside the molten pool or due to the presence of gas bubbles in the powder, that is later released as bubbles after cooling and solidification (Dutta et al., 2019, pp. 32-35). Some materials are more susceptible to gas absorption during the melt process than others (Milewski, 2017, p. 238). Excessive energy density results in entrapped gas pores (A. Fatemi et al., 2020). Controlling the porosity is important to the mechanical properties of the component.

2.5.2. Lack of fusion (LOF) voids

To secure good part quality in AM processes, bonding between layers is a very important factor. The incomplete bonding or lack of fusion between successive layers can lead to void formation and this void formation can result in delamination between layers, leading to inferior mechanical properties. These voids are not spherical in shape and are normally bigger than gas porosity, because of this, voids are more harmful than gas porosity (Dutta et al., 2019, pp. 35-38).

The void formation between layers is one of the principal disadvantages of AM parts and depends primary on the AM method and the material used (Ngo et al., 2018, p. 189). It can be the result of insufficient heat input to melt the underlaying layer creating a lack of bounding between the two consecutive layers. Therefore it is important to have a proper selection of process parameters (DebRoy et al., 2018, p. 135; Dutta et al., 2019, pp. 35-38).

The printing orientation can also play an important role in minimizing the damage of LOF defects. “If the part is built in a way that the defects are oriented in the most favorable orientation with respect to the loading direction” the harmful effect of LOF defects could be minimized (A. Fatemi et al., 2020).

2.5.3. Loss of alloying elements

When the molten pool temperatures are very high, due to high energy density of the heat source (laser or electron beam), loss of alloying elements takes place. This can cause changes in the chemistry of the final product, affecting the mechanical properties, physical properties and quality components (DebRoy et al., 2018, p. 133; Dutta et al., 2019, p. 31).

2.5.4. Cracks

In AM processes the high cooling rates can lead to cracks in the metal due to solidification shrinkages, so reducing this cooling rates can help on reducing these cracks (Dutta et al., 2019, p. 39). Porosity can also be a site for crack initiation (Yuan, 2019).

2.5.5. Microstructural heterogeneity

The microstructure of AM parts cannot be generalized since they are dependent on the material and the process parameters used. Among the process parameters that affect the microstructure we can mention:

- Scanning speed (in PBF processes).
- Traverse speed (in DED processes).
- Energy density (power).
- Gas flow rate.
- Machine chamber environment.
- Build plate temperature (Dutta et al., 2019, pp. 30, 93).

During AM processes, formation of heterogeneous microstructural bands and segregation occurs due to the redistribution of solute particles as several layers are deposited. These bands are known as heat affected zone (HAZ). Solidification cooling rates influence the amount of solute segregation inducing to microstructural heterogeneity (Dass & Moridi, 2019, p. 9).

2.6. Residual stress in additive manufactured metal parts

One disadvantage of the AM technologies is the finding of residual stresses because these negatively impact the mechanical properties of the final product. The melting process generates temperature gradients between the layers which lead to important residual stresses (A. Fatemi et al., 2020; Zadi-Maad et al., 2018). These rapid and repeated changes in temperature along with fast solidification are the main sources of residual stress during the AM processes (Dutta et al., 2019, p. 40; A. Fatemi et al., 2020; C. Li, Liu, Fang, & Guo, 2018). "Laser power, laser scanning speed, powder feeding rate, and scanning strategy are the main process and design parameters that can affect the thermal history, microstructure, and level of residual stresses within the fabricated component" (Dutta et al., 2019, p. 40). Therefore, planning and controlling these fabrication process parameters can reduce the residual stresses. Post process treatment can also reduce residual stresses in metal AM parts (A. Fatemi et al., 2020; C. Li et al., 2018). Residual stresses in metal AM parts can result in distortion (Brandt, 2016, p. 64), cracking and delamination (Brandt, 2016, p. 64; Dutta et al., 2019, p. 40).

2.7. Fatigue in additive manufactured metals

Metal fatigue is a weakening and breaking of a metal part subjected to cyclic loading. In the first stage of the metal fatigue, micro-cracks begin to form on the metal. These micro-cracks continued to be stressed by cycling loading, leading to large crack initiation and propagation, which may result in metal failure. Therefore, crack propagation controls the fatigue life of the metal parts.

Irregular surface conditions on the AM metal part create stress concentration locations and are potential cause for crack initiation which can lead to fatigue during service (A. Fatemi et al., 2020).

Recent studies have been performed to investigate the fatigue behavior of different AM materials such as titanium alloys (A. Fatemi et al., 2020; Ali Fatemi, Molaei, Sharifimehr, Shamsaei, & Phan, 2017; Ali Fatemi et al., 2019; Reza Molaei & Fatemi, 2019; R. Molaei et al., 2020; Pegues et al., 2020; Prabhu, Vincent, Chaudhary, Zhang, & Babu, 2015), aluminum alloys (Tang & Pistorius, 2019; Yang et al., 2018), nickel-based super alloys (Johnson, Shao, Shamsaei, Thompson, & Bian, 2017) and various grades of stainless steels (Alsalla, Smith, & Hao, 2018; Elangeswaran et al., 2019; A. Fatemi et al., 2020; Reza Molaei & Fatemi, 2019; Nezhadfar et al., 2019; Yadollahi, Shamsaei, Thompson, Elwany, & Bian, 2017). The factors found to have mostly affected the mechanical and fatigue behavior of additive manufactured parts in these studies were the porosity, lack of fusion, surface roughness, microstructural heterogeneity, and anisotropy.

Since researchers have tied the variations of fatigue properties to the defects, and microstructure of the AM parts (Dass & Moridi, 2019; Dutta et al., 2019, p. 119), and each of these has its own distinct effect on the properties of the final product, it is important to better understand the fatigue behavior of AM metals considering these manufacturing parameters.

Published fatigue data of AM Ti-6Al-4V samples fabricated by Electron Beam Melting (EBM - a DED-EB process) that have undergone different postprocessing treatments was collected and reviewed by a recent study (Chern et al., 2019). The authors concluded that all the AM samples that were subjected to HIP postprocess and machining showed very good fatigue properties. After these the next best fatigue properties were shown by the samples that were subjected only to machining. The samples that were subjected only to HIP post processing

showed poor fatigue properties in comparison with samples that were subjected only to machining. Finally, the sample that did not undergo any postprocessing or machining showed the poorest fatigue properties.

Another study (Prabhu et al., 2015) on AM Ti-6Al-4V samples produced by LENS (a DED-L process) has shown that the fatigue life of these parts was mainly controlled by physical defects. They studied the fatigue behavior of the LENS AM Ti-6Al-4V samples in the as built condition and analyzed how the microstructure and physical defects influenced the fatigue performance. They observed that the fatigue life of the samples was affected by the presence and location of the unmelted particles (unmelted particles lead to stress concentration). It was observed that the location of the crack initiation was determinant of the fatigue life. The samples with crack initiation located at the surface had lower fatigue life than those with crack initiation in the bulk. They concluded that the as built AM Ti-6Al-4V samples produced by LENS processes can have a fatigue life comparable to wrought material.

Spierings et al. (2013) studied the fatigue performance of additive manufactured SS316L and 15-5 PH stainless steel fabricated by the SLM process (a PBF-L process). The samples were printed in vertical orientation, meaning layer planes perpendicular to the load axis of the specimens. The study compared the dynamic mechanical properties of these two types of stainless steel with similar conventional fabricated materials. The results showed the fatigue life for SLM SS316L to be 25 per cent lower than conventional fabricated material and for SLM 15-5 PH to be 20 per cent lower than conventional fabricated material. At higher stress amplitude the fatigue life of SLM SS316L is comparable to the conventional fabricated material, but for SLM 15-5PH the fatigue life is lower than conventional fabricated materials. The influence of surface quality was also studied for SLM 316L and it was found that polishing improves the fatigue life but at higher stress amplitudes the fatigue behavior of SLM SS316L was similar to the as-fabricated material.

Blinn et al. (2018) investigated the influence of heat treatment on the microstructure and fatigue behavior of AM SS316L specimens fabricated by Selective Laser Melting (SLM - a PBF-L process) and Laser Deposition Welded (LDW - a DED-L process). Experimental results show that the heat treatment does not influence significantly the anisotropic fatigue behavior of the AM specimens.

The influence of post-treatments on the fatigue behavior of AM SS316L fabricated by PBF-L was investigated by Elangeswaran et al. (2019). It was found that AM specimens subjected to machining have better fatigue behavior compared to the traditionally manufactured 316L. This was true with and without stress relief heat treatments.

Poulin et al. (2020) studied the fatigue strength of AM Inconel 625 manufactured by PBF-L process. Porosity was planted intentionally in the gauge section of the samples and annealing heat treatment was applied. Based on the results of this experiment they concluded that the amount of porosity reduces the fatigue resistance of the PBF-L AM Inconel 625. They also concluded that the fatigue behavior of PBF-L AM parts cannot be only related to the amount of porosity but to the geometry and size of individual defects.

Zhai et al. (2016) investigated LENS (a DED-L process) and PBF-EB manufactured Ti-6Al-4V alloys. They concluded that LENS and PBF-EB manufactured Ti-6Al-4V alloys are stronger than their wrought counterpart but less ductile. Post-LENS heat treatment and post PBF-EB heat treatment improves the mechanical properties of the part. Fabricated LENS Ti-6Al-4V and PBF-EB Ti-6Al-4V yield lower fatigue crack growth threshold than wrought Ti-6Al-4V but higher fracture toughness.

Fatemi et al. (2019) investigated the fatigue behavior of AM Ti-6Al-4V. In the investigation the effects of defects, surface finish, residual stresses, geometry, size, heat treatments, as well as different loading direction were considered. Fabrication process-induced defects, such as porosity and lack of fusion voids, were found to significantly affect the fatigue behavior of AM metals. The irregular shape of lack of fusion voids causes larger stress concentration making them more harmful than the spherical entrapped gas pores. Hot isostatic pressing (HIP) reduces the amount and size of the defects. The AM processes involve high thermal gradients, high energy density and fast solidification, this results in the formation of residual stresses which influence the fatigue behavior. Residual stresses can be reduced by using proper fabrication process parameters, proper layer orientation and post fabrication heat treatments. Surface roughness is higher in the as-built AM parts compared to their traditional manufactured counterparts. Surface roughness is controlled by the powder size, layer thickness, geometry of the part, manufacturing process type, manufacturing process parameter, and orientation. Machining improves the fatigue performance of AM parts since fatigue cracks generally initiate from the surface of the as-built AM parts. Layer orientation can be a key factor in the fatigue performance of AM parts. Specimens built perpendicular to their loading direction

(layer planes parallel to the load axis of the specimen) have normally longer fatigue lives compared to the specimens built parallel to their loading direction (layer planes perpendicular to the load axis of the specimens). This is due to the fact that lack of fusion defects are usually perpendicular to the build direction. It is important to mention that HIP treatment has a significant effect if the AM parts undergoes machine treatment as well.

The fatigue properties of diverse types of steel manufactured by SLM (a PBF-L process) was investigated by (Afkhami et al., 2019). Parameters such as build orientations, post-processing heat treatment and surface quality, which are recognized to influence the fatigue behavior of these steels were reviewed. Table 5 (Afkhami et al., 2019) shows the diverse types of SLM steels presented in this study. The results from the reviewed studies have shown that building orientation significantly influences the fatigue life of SLM steels. SLM steel specimens with building direction perpendicular to their loading direction as shown in Figure 10, have superior mechanical properties compared to the SLM steels with building direction parallel to their loading direction. SLM steel parts printed with the building direction perpendicular to the loading direction, showed higher distribution of porosity with smaller diameter compared to the SLM steel parts printed with the building direction parallel to the loading direction. This was due to the fact that the ones printed with the building direction perpendicular to the loading direction, faced higher cooling rates and faster solidification.

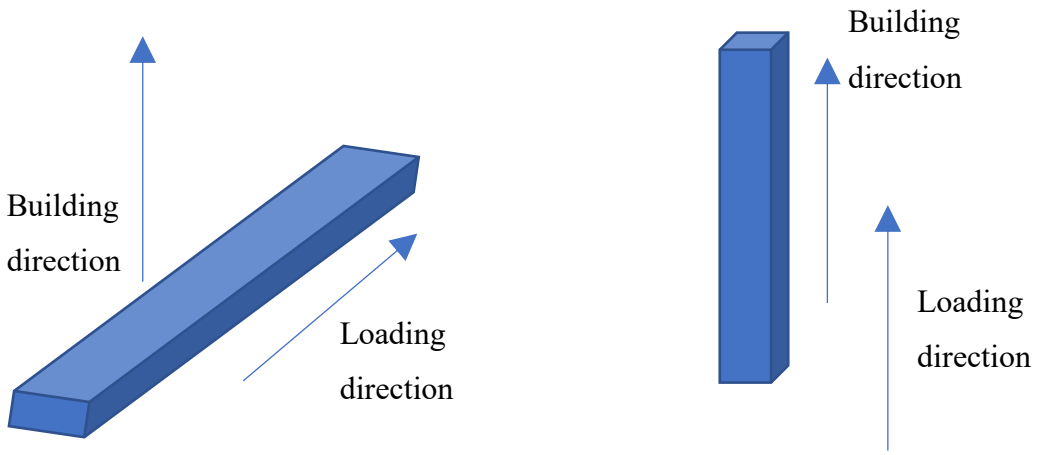

Figure 10: Building direction.

Table 5: List of SLM steels present in the fatigue studies (Afkhami et al., 2019).

Name of steel according to:			
Commercial	EOS	UNS	Others
316L	316L	S31673	EN1.4401
18Ni-300	MS1	K93120	EN1.2709
15-5 PH	PH1	S15500	–
630	17-4 PH	S17400	17Cr-4Ni; AISI630; EN1.4542
300M	–	K44220	4340M
H13	–	T20813	DIN1.2344
Marlok® C1650	–	–	–

The research showed that a proper selection of heat treatment improves the mechanical properties of SLM steel, and surface machining improves the fatigue strength of SLM steels. However, improving the surface roughness releases substrate compressive residual stress near the surface which leads to crack initiation and propagation. In general, the research has shown that the fatigue properties for low or medium strength steel fabricated using SLM process with a proper selection of process parameters, heat treatment and surface machining, can be as good as the conventionally manufactured steels. However further studies are required for ultra-high and high strength steels.

3D printed metals by the SLM process have shown inferior fatigue strength in comparison to their wrought counterparts despite their building direction (Blinn et al., 2018; Liverani, Toschi, Ceschini, & Fortunato, 2017; Miroslav, Pavĺna, Jana, Pavel, & Boiviek, 2017; Yadollahi et al., 2017).

The fatigue cracking behavior of AM Ti-6AL-4V and 17-4 PH stainless steel specimens fabricated by two PBF-L processes, and a comparison with their wrought counterparts was studied by Molaei & Fatemi (2019). The cracking mechanisms were studied under different conditions such as annealing, HIP, surface roughness, build orientation and different built parameters. Their specimens were tested in the as built condition and machined condition. The following Table 6 (Reza Molaei & Fatemi, 2019) resumes the observations of the failure mechanisms of all the specimens tested.

Table 6: Failure mechanisms of the PBF-L AM 17-4 PH Stainless Steel, PBF-L AM Ti-6Al-4V and wrought specimens under different conditions (Reza Molaei & Fatemi, 2019).

Summary of the failure mechanisms of the wrought and AM specimens under different conditions.

				Unnotched					Notched	
				Wrought	AM Machine #1		AM Machine #2		AM Machine #1	
	Condition	Surface Finish	Build Orientation	LCF & HCF	LCF	HCF	LCF	HCF	Initiation	Growth
Ti-6Al-4V	Annealed	As-Built	Vertical				Shear	Tensile		
	Annealed	Machined	Vertical			Tensile	Shear	Tensile		
	Annealed	Machined	45°		Shear	Tensile				
	HIPed	As-Built	Vertical		Shear	Tensile	Shear	Tensile		
	HIPed	Machined	Vertical		Shear	Shear				
	HIPed	Machined	45°		Shear	Shear			Shear	Tensile
	Annealed	Machined		Shear						
17-4 PH	H1025	As-Built	Vertical		*	*			Tensile	Tensile
	H1025	Machined	Vertical		Shear	Shear			Shear	Tensile
	H1025	Machined		Shear						

Note: LCF here refers to fatigue lives shorter than about 20,000 cycles and HCF to longer than 20,000 cycles.
* Failure due to the fabrication defect networks on the surface.

Among the findings in this research on the two metallic AM materials we can mention:

The failure mechanism of the AM metals depends on the surface defects, internal defects and microstructure. Surface machining proves to be able to remove surface defects and change crack path, the failure mechanism and the fatigue life. The cracking behavior of the AM metals also depend on the surface defects, internal defects and microstructure. The use of HIP shrinks the internal defects and transforms the microstructure to a more ductile structure, but HIP processes are effective when the rough surface is removed, because the main contributors in controlling the cracking behavior (crack initiation and growth direction) are the stress concentration effect of surface roughness. Proper selection of post treatment processes and/or process parameters reduce the anisotropy effect on cracking behavior and fatigue performance.

For AM specimens under notched condition, the cracking behavior is controlled by stress concentration and not by defects, similar to the wrought material.

The fatigue performance of PBF-L AM Ti-6Al-4V was studied by Molaei et al. (2020). The effect on the microstructure of process parameters and post treatments were discussed. It was shown that variating the process parameters affects the failure mechanism and the fatigue behavior of the PBF-L Ti-6Al-4V part by affecting the microstructure, the surface quality, the defect and the residual stresses. Surface machining is important in improving the fatigue behavior by removing surface defects and their stress concentration effects. Appropriate selection of process parameters and post fabrication processes may improve the fatigue performance. Fatigue behavior was dominated by microcracks.

The fatigue behavior of 17-4 PH stainless steel produced by SLM (a PBF-L process) was investigated by Yadollahi et al. (2017). The effects of building orientation and heat treatment were considered. It was found that the fatigue strength of SLM 17-4 PH stainless steel is lower than that of its wrought counterpart. Heat treatments increase its tensile strength comparable to its wrought counterpart. Heat treatment improves the fatigue behavior in low cycle fatigue (LCF) performance but in high cycle fatigue (HCF) performance the heat treatment has detrimental influence. Building orientation influences the fatigue behavior of SLM 17-4 PH stainless steel. Parts built vertically orientated (defects formed between layers orientated perpendicular to the load direction) as shown in Figure 11, present lower fatigue strength than parts built horizontally orientated (defects formed between layers orientated parallel to the load direction) as shown in Figure 11. Defects caused by the unmelted region, were found to be the most dangerous defects on the fatigue strength of SLM 17-4 PH stainless steel. Cracks initiated from unmelted regions.

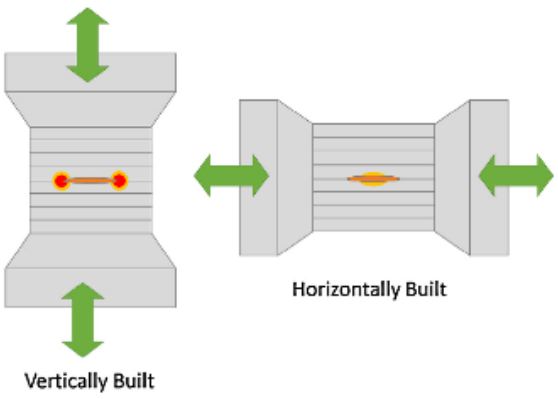

Figure 11: Built orientation with respect to the defect formed during fabrication

Carneiro et al. (2019) performed experiments to study the fatigue life of 17-4 PH stainless steel fabricated by SLM and conventionally manufactured 17-4 PH stainless steel. Both sets of specimens were built with identical shape, were subjected to the same post-manufacturing heat treatment and surface treatment. The results were compared. It was observed that pores, in SLM 17-4 PH stainless steel, decrease its fatigue strength in the high cycle fatigue regime compare to the conventionally manufactured 17-4 PH stainless steel. Lower ductility in SLM 17-4 PH stainless steel compared to conventional manufacture 17-4 PH stainless steel was also observed due to internal defects and un-melted particles.

The fatigue failure mechanism varies in AM metals. Even using the same AM fabrication process and a specific metal, the failure fatigue mechanism varies depending on the chosen process parameters and the used post process treatments (A. Fatemi et al., 2020).

Since fatigue cracks regularly start form the surface, it is important to pay special attention to the surface roughness of AM metal parts while investigating their fatigue behavior (A. Fatemi et al., 2020). In an investigation of published fatigue data on AM Ti-6Al-4V fabricated with different AM processes (P. Li, Warner, Fatemi, & Phan, 2016), it was concluded that surface roughness leads to low fatigue performance and therefore AM Ti-6Al-4V requires surface treatment to achieve fatigue performance superior to wrought and annealed Ti-6Al-4V.

To understand the fatigue behavior of AM metals, the effect of defects, geometry, residual stresses, heat treatment, layer orientation and surface finish must be considered. (Ali Fatemi et al., 2019). A more conclusive understanding of the fatigue behavior in this field is needed to establish accurate prediction of fatigue properties in AM parts (Ali Fatemi et al., 2019). The proper processing parameters and build orientation, as well as post process heat treatment, could improve the fatigue performance by decreasing the residual stresses generated during the fabrication process.

2.8. Post AM fabrication Processes

Metal AM parts generally suffer from defects, including internal defects and surface defects, these defects are known to influence the fatigue performance. Therefore, post processing operations and finishing operations are very often required for metal AM parts to get the desired surface condition, uniform microstructure, for stress relief and to fully develop the desired properties (Milewski, 2017, pp. 146, 230).

Rough surface and microcrack on the surface, can be reduced by a surface finish operation. Surface finish operations may include grinding, peening, sanding or polishing (Milewski, 2017, p. 231).

Post process treatments help to improve the mechanical properties of AM metal parts (Milewski, 2017, p. 140). HIP processing or heat treatment such as annealing, homogenization, recrystallization or precipitation hardening, can be used to eliminate or reduce thermal stresses, homogenize microstructure, or modify mechanical properties (Milewski, 2017, pp. 67, 140). Fatigue performance can also be improved by HIP and post-process heat treatment (Dutta et al., 2019, p. 120; Milewski, 2017, p. 160). HIP process reduces the porosity by closing the internal pores, voids and homogenizing the microstructure (Dutta et al., 2019, p. 120; P. Li et al., 2016). Machining can be used to minimize the surface roughness, which reduce the stress concentration (Dutta et al., 2019, p. 120). "Heat treatments remove residual stresses" (P. Li et al., 2016).

During heat treatment (HT) the AM part is exposed to high temperatures in an inert or vacuum furnace at heating cycles below the melting point for a period of time of 2 to 4 hours (Milewski, 2017, pp. 67, 233). During hot isostatic pressing (HIP) the part is exposed to high temperatures below the melting point and high gas overpressures at pressures of 100s of MPa for a period of time of 2 to 4 hours.

2.9. Composition of AM 17-4 PH Stainless Steel

17-4 PH stainless steel is a martensitic precipitated hardened (PH) stainless steel widely used in the aerospace, petrochemical and general metalworking industries thanks to its good corrosion resistance and excellent mechanical properties (Carneiro et al., 2019; A. Fatemi et al., 2020). It is the most used of all the precipitation-hardening stainless steels (AK Steel; Mirzadeh & Najafizadeh, 2009). For this thesis, a 3D printer from Markforged was used, specifically a Markforged Metal X. Table 7 shows published 17-4 PH stainless steel composition values and Table 8 shows published 17-4 PH stainless steel mechanical properties for as-sintered BMD, all values provided by the printer manufacturer (Markforged, 2021).

Table 7: Composition of AM 17-4 PH Stainless Steel. Adapted from *(Markforged, 2021).*

COMPOSITION		Weight Percent (wt. %)
Carbon	C	0.07 maximum
Manganese	Mn	1.00 maximum
Phosphorus	P	0.04 maximum
Sulfur	S	0.03 maximum
Silicon	Si	1.00 maximum
Chromium	Cr	15.00 – 17.50
Nickel	Ni	3.00 – 5.00
Copper	Cu	3.00 – 5.00
Niobium	Nb	0.15 – 0.45
Iron	Fe	bal

Table 8: Typical mechanical properties of Markforged 17-4 PH Stainless Steel samples as-sintered fabricated by the BMD method (Markforged, 2021).

Typical Mechanical Properties	Standard	As Sintered
Ultimate Tensile Strength	ASTM E8	1050 MPa
0.2% Yield Strength	ASTM E8	800 MPa
Elongation at Break	ASTM E8	5%
Tensile Modulus	ASTM E8	140 GPa

2.10. Material tests

This section presents the theory of the test performed in this project.

2.10.1. Tensile test

One of the most common used methods to determine the properties of metallic materials is the tensile test. The test determines how a material reacts to forces applied in tension. The tensile test provides fundamental properties and is fast, easy to perform and relatively cheap.

Tensile test:

The tensile test process as described by Davis is such as (Davis, 2004, pp. 33-47):

A tensile test is a test where a pulling force (a load) is applied on opposites ends of a specimen until the specimen breaks. The test provides information about the tensile strength, yield strength, ductility (percent elongation and reduction in area), and other properties of the metallic material unique to the specimen. A tensile specimen is typically a standardized sample cross-section. It has enlarged ends for gripping and a gage section with reduced cross-sectional area.

The test consists of placing the test specimen in the testing machine and extending it slowly until it fractures. As the axial load increases, the elongation of the gauge section is recorded against the applied force.

From these load-elongation measurements made on the test specimen, an engineering stress-strain curve profile is obtained as the material is being pulled until breakage. The engineering strain, *e*, used in this engineering stress-strain curve, is calculated using the instant change in length of the gage section compared to the original length of gage section:

$$\text{Engineering strain} \qquad e = \frac{\Delta L}{L_0} = \frac{L - L_0}{L_0}$$

where ΔL is the change in gauge length and L_0 is the initial gage length.

The strain can also be expressed as true strain ε, and is based on the instantaneous gage length of the specimen while the test is in progress divided by the original length of the gage section of the specimen:

$$\text{True strain} \qquad \varepsilon = \ln\left(\frac{\mathrm{L}}{L_0}\right) \qquad \text{where L is the instantaneous length}$$

The engineering stress, or nominal tress, *s*, used in this engineering stress-strain curve, is calculated dividing the force measurements at any time during the test by the original area of the cross section of the gage section of the specimen (A_0):

$$\text{Engineering stress} \qquad s = \frac{F}{A_0}$$

where F is the tensile force and A_0 is the initial cross-sectional area of the specimen gage section.

The stress can also be expressed as true stress σ, and is based on the force at any time during the test divided by the instantaneous cross-sectional area of the gage section of the specimen (A) while the test is in progress:

$$\text{True stress} \qquad \sigma = \left(\frac{\mathrm{F}}{\mathrm{A}}\right)$$

After the force-elongation data are converted to engineering stress and strain, an engineering stress-strain curve from a tensile test can look like the following Figure 12 (Davis, 2004, p. 14).

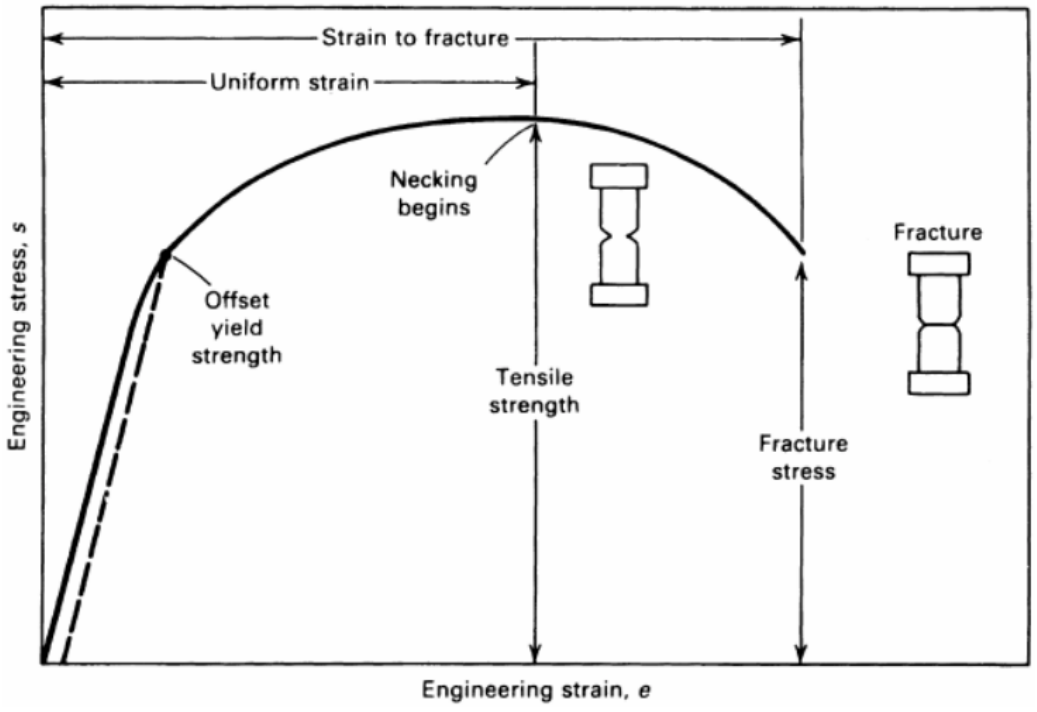

Figure 12: Engineering strain-stress curve (Davis, 2004, p. 14).

Young's modulus (E):

In the initial part of the tensile test (elastic region) the relation between stress and strain is linear for most materials. The relationship is defined as Hooke's law. The slope of this initial linear

portion represents the modulus of elasticity, or Young's modulus, *E*. The modulus of elasticity, *E*, quantifies a material's resistance to elastic deformation, and is a measure of the stiffness of the material. The modulus of elasticity is determined using the formula:

$$\text{Young's modulus} \qquad \mathrm{E} = \frac{s}{e}$$

In the elastic region the material does not plastically deform. If the load is removed, the material will come back to its original length. E only applies in the linear region of the curve: E is the slope of the line in the linear region.

Yield strength:

Yield strength is the magnitude of the stress corresponding to the yield point at which the material ceases to be elastic and begins to deform plastically. After this point if the load or stress is removed the specimen will remain permanently deformed. This point is called the Elastic Limit. For metals, it is difficult to define an exact yield point. Therefore, an offset method is used to determine it. According to ASTM E8, this is done by drawing a line parallel to the straight-line (elastic region) of the stress-strain curve at 0.2% of the plastic strain. The stress at the point where this line intercepts the curve gives the yield strength by the offset method.

Ductility:

The measures of ductility usually obtained from the tension test are the engineering strain at fracture or elongation (e_f), and the reduction in area at fracture or stretch (RA). Both of these properties are normally expressed as a percentage.

$$\%e_f = \frac{L_f - L_0}{L_0} * 100$$

where L_f is the final gage length, the length of the gage section at fracture and L_0 is the initial gage length.

$$\%RA = \frac{A_0 - A_f}{A_0} * 100$$

where A_0 is the initial cross-sectional area of the specimen gage section and A_f is the final cross-sectional area of specimen gage section.

Ultimate Tensile Strength (UTS):

The ultimate tensile strength is the largest load that a specimen sustains during the test before fracture. It is not necessarily the strength at fracture, it depends on the material. As we can see in Figure 12 (Davis, 2004, p. 14) the strength at fracture is lower that the UTS.

Test parameters:

Test parameters will be according to ASTM E8/E8M.

2.10.2. Optical Light Microscopic technique

The light microscope, also referred to as optical light microscope (OLM), is an excellent tool for the study of the material's microstructure that is not visible to the naked eye. The OLM usually uses visible light and a system of lenses to achieve the wanted magnified images of the specimen. The images form the microscope can be observed with the eye directly or can be recorded by computer, video or photographic techniques. With the light microscope the microstructure of metal samples can be studied (Holgate & Webb, 2003).

To reveal the important details of the microstructure of the specimens, preparation of the surface of the sample is needed. The surface of the sample must be ground and polished using finer abrasive papers and powders until a shiny surface finish is reached.

The light microscope allows to view objects at a 1000x their original size.

3. EXPERIMENTAL DETAILS

Experimental work has been conducted in order to investigate the effect of building orientation on the microstructure and mechanical properties of 17-4 PH stainless steel fabricated within a BMD process under monotonic load.

The specimens were produced by the metal 3D printing system available at the University of Stavanger, which uses a material extrusion technology. The 3D printer used was a Markforged Metal X. Test samples were fabricated from 17-4 PH stainless steel. The experiments were performed at the machine and microscopy labs at the university of Stavanger.

A CAD software was used to create the 3D model of the specimens. This file was converted into STL-file. An STL file contains 3D information about the part and is the type of file regularly used by additive manufacturing machines. The STL file was uploaded to Markforged Eiger 3D system software, which is the 3D printing preparation software (slicer software) developed by Markforged. The slicer software slices the model into thin layers and gets the model ready for printing. This software generates information about the number of layers, the layer thickness, the tool path, the temperature, among others. The material was then selected as well as the printing orientation of the specimens. Finally, the specimens were printed, washed, and sintered.

The following tests were performed on the as-sintered additive manufactured 17-4 PH stainless steel specimens:

- Tensile test
- Macrostructure evaluation using an optical light microscope

From the tensile test, the ultimate tensile strength (UTS), yield tensile strength (YTS), Young´s modulus (E) and elongation (%) were obtained, and the results were compared to the Markforged AM 17-4 PH stainless steel as-sintered values. Table 8 (page 40) presents the Markforged test values for the as-sintered 17-4 stainless steel. The optical light microscope was used for optical analysis of the macrostructure of the samples.

The experiments were performed following the standards and HMS regulations at the University of Stavanger labs. A full detail of the experimental methods used are explained next.

3.1. Description of the AM technology used to manufacture the samples

The 3D printer Markforged Metal X, produced by Markforged, used to produce the additive manufactured 17-4 PH stainless steel specimens uses a material extrusion technology known as BMD.

The system consists of a printer, a debinder, and a furnace, which are integrated with a web-based software. In these processes, metal rods (metal powder bound in plastic) are fed through a heated extruder on top of the build tray. This shapes the part layer by layer. Once the print is complete, the part is transferred to the debinder, where the part is immersed in fluid (metal solvent) to dissolve the primary binder material. In this second stage of the process the primary binder is removed creating an open pore structure all over the part in preparation for sintering. Once the cycle is completed the part goes into the sintering furnace. In the furnace the part is heated to temperatures near melting, eliminating the remaining binder. This causes the metal particles to fuse together going from metal powder to a metal part (Desktop Metal, 2021).

3.2. Sample manufacturing

The samples used in this study were fabricated with 17-4 PH stainless steel wire supplied by Markforged. The specimens were produced with a Markforged Metal X system machine which has a maximum build volume size of 300 mm x 220 mm x 180 mm. The machine is provided with sets of parameters for the different materials. The dimension of the samples for the tensile test were according to ASTM E8/E8M subsize specimen (ASTM international, 2021b) as shown in Figure 13 (all dimensions are in mm). Gauge length of the specimens, G = 25 mm. The samples were tested in an as-sintered condition.

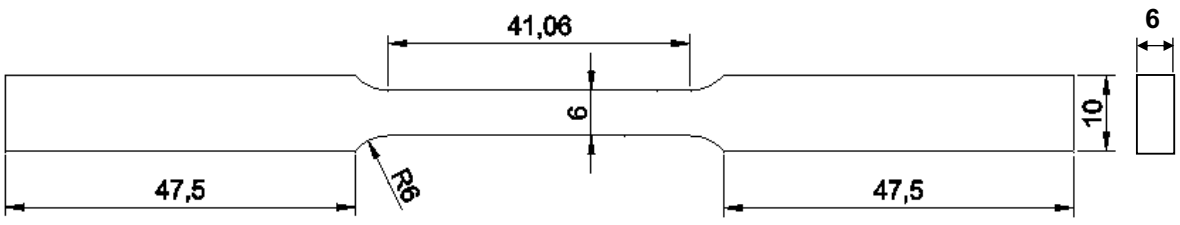

Figure 13: Standard tensile bar with dimension according to ASTM E8/E8M.

For the tensile test three groups of three specimens each were manufactured. The first group contained horizontally oriented specimens, which were named XY-flat 1, XY-flat 2 and XY-flat 3. These specimens were built after 68 layers. The second group contained horizontally oriented specimens that were rotated in a way to create the necessity of a support structure during the printing process, these specimens were named XY-sided 4, XY-sided 5 and XY-sided 6 and were built after 100 layers. The third group contained vertically printed specimens which were named ZX 7, ZX 8 and ZX 9. These specimens were built after 1175 layers. The building directions of the specimens XY-flat, XY-sided, and ZX are shown in Figure 14, Figure 15, and figure 16 respectively.

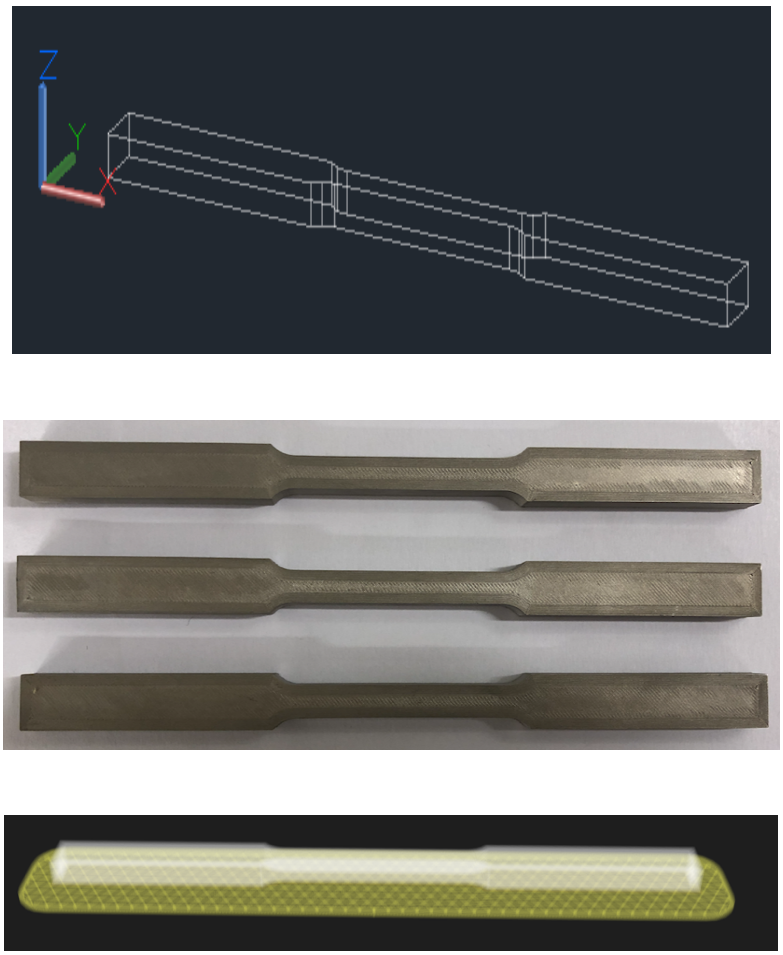

Figure 14: BMD tensile testing sample manufactured at the XY-flat building orientation.

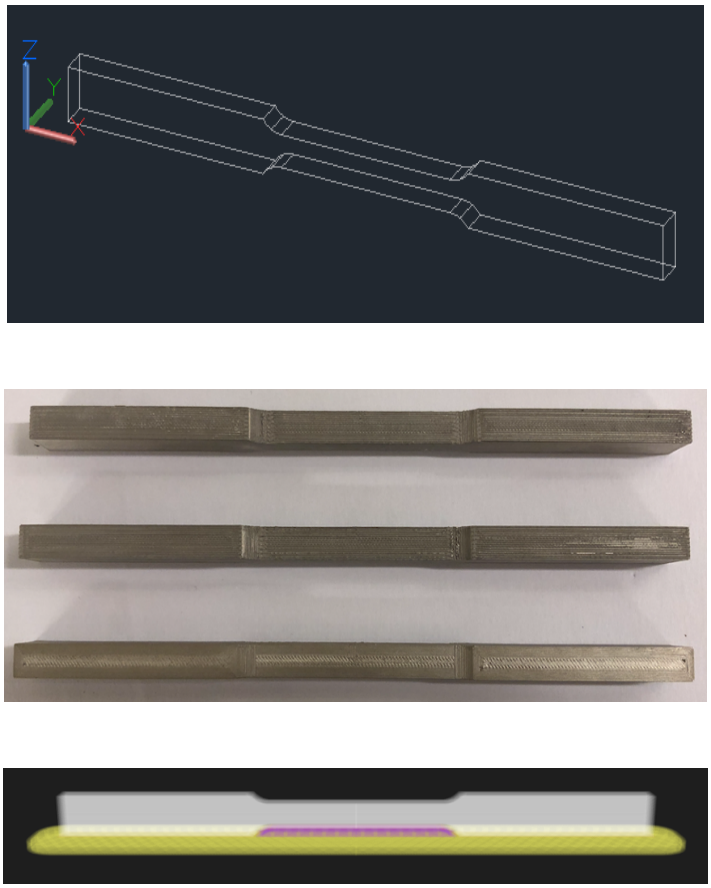

Figure 15: BMD tensile testing sample manufactured at the XY-sided building orientation.

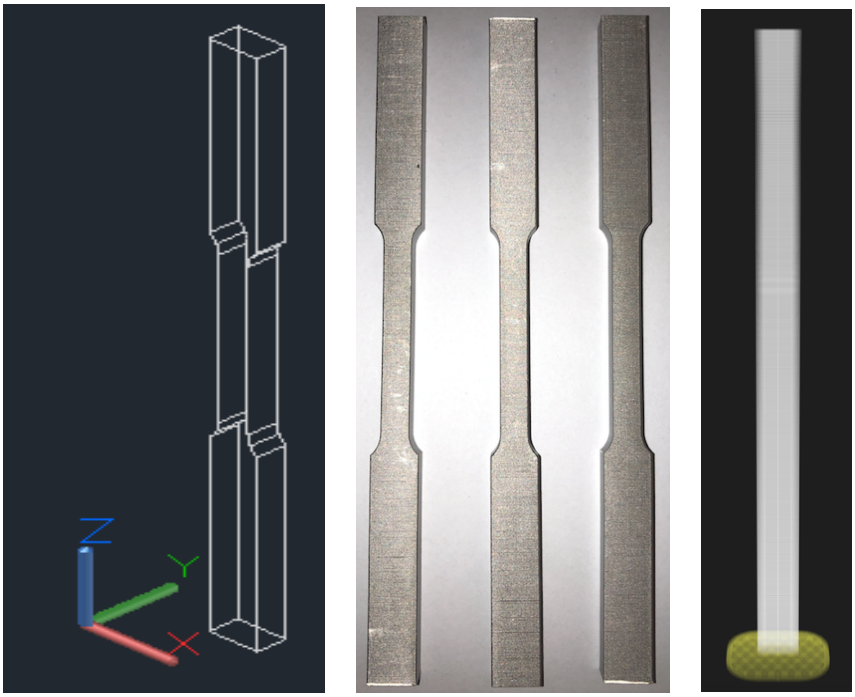

Figure 16: BMD tensile testing sample manufactured at the ZX building orientation.

For the optical light microscope two bar samples where produced, one bar built in the vertical direction (V) (10 mm x 10 mm x 50 mm) and one bar built in the horizontal direction (H) (10 mm x 50 mm x 10 mm) as shown in Figure 17.

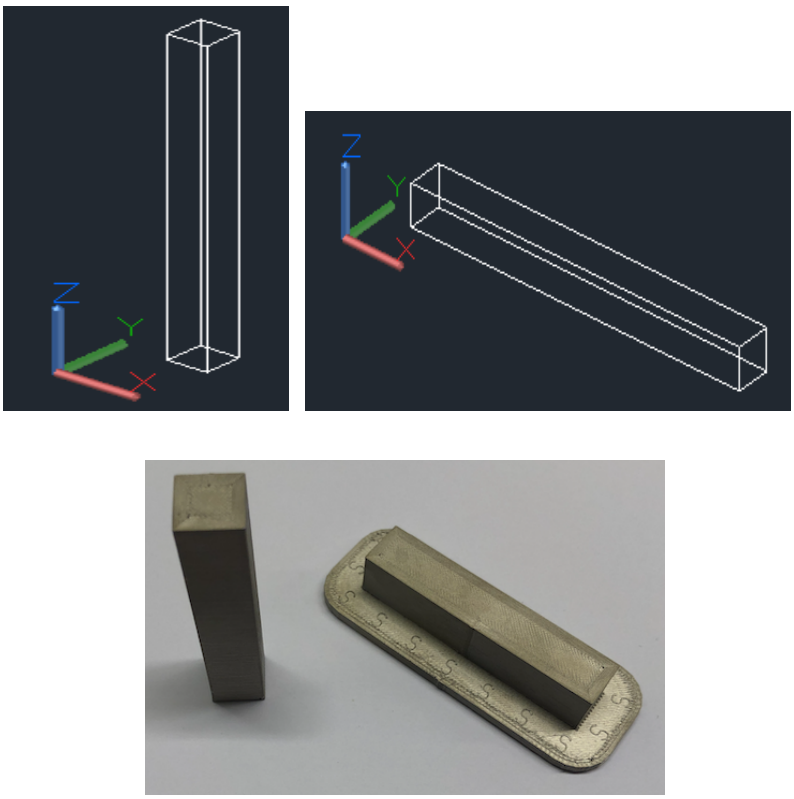

Figure 17: Illustration of the 2 building directions V and H.

Figure 18 shows the raster strategy for an XY-flat subsize tensile specimen. The seven-perimeter raster and 45° solid infill can be seen. For alternating layers, the infill angle alternated at ± 45°. The filament was initially deposited along the component edge and then the inner part of the component was filled by inclined raster. After the completion of the first layer, the process was repeated to generate all the other layers.

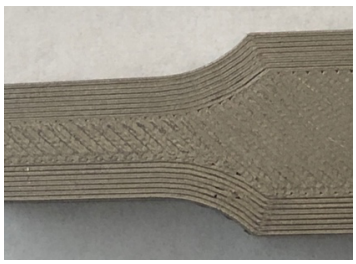

Figure 18: Raster strategy for an XY-flat subsize tensile specimen.

3.3. Sample preparation for OLM

The samples used for microstructural investigation using the OLM required special metallographic preparation.

- Small specimens were cut using a Struer Discotom-5 machine. After cutting, the specimens were cleaned, rinsed and dried.
- The specimens were labeled with 2 letters and a number. The first letter indicates if the sample was vertically printed (V) or horizontally printed (H) the second letter indicates if the view was parallel to the layers plane direction, top view (T), or perpendicular to the layers plane direction, side view (S) and the number indicates the specimen number. For example, the first sample taken from the vertically printed specimen with the face analyzed parallel to the layers plane direction was named VT1 and the first sample taken from the vertically printed specimen with the face analyzed perpendicular to the layers plane direction was named VS1.

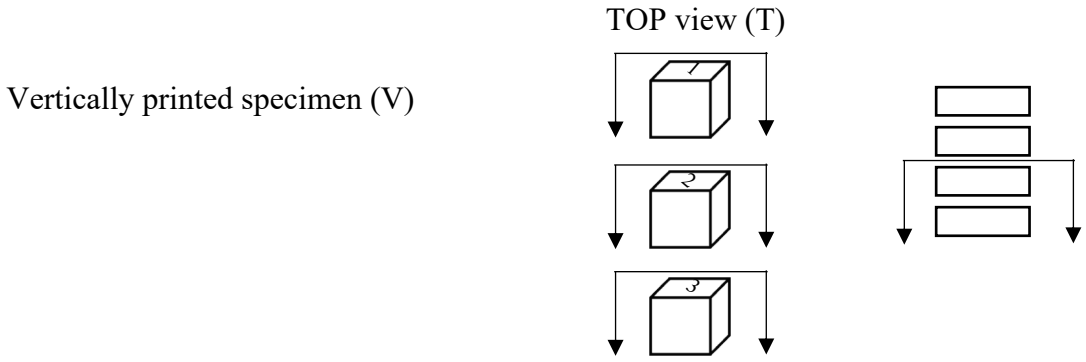

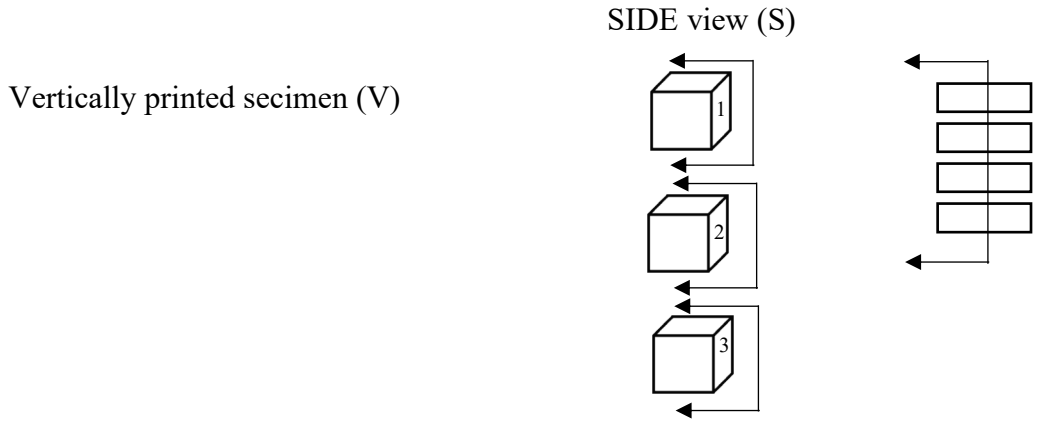

- To make easier the handling of the specimens while polishing and grinding, they were mounted in resins. A Struers CitoPress-30 machine was used to mount the specimens. The Multifast method was selected on the Struers Cito press-30 machine. One layer of on-conductive plastic Multifast was used. A release antistick agent was added to the machine to make sure the plastic did not stick to the machine. A total of nine specimens were prepared. Figure 19 shows a specimen mounted in the black resin.

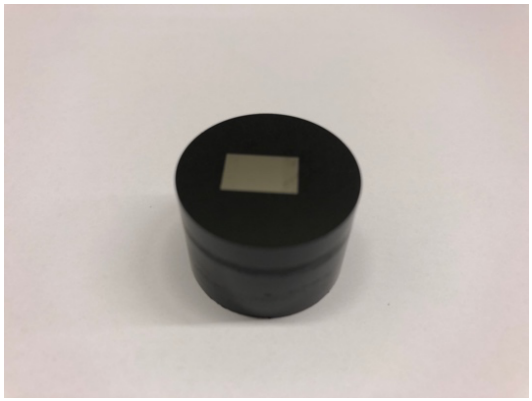

Figure 19: Specimen mounted in transparent resin.

- The specimens were subjected to progressive grinding and polishing in several stages according to Struers standards procedures for preparing stainless steel. The grinding and polishing were performed on a Struers TegraPol-35 machine. The method D from the Struers TegraPol-35 machine consisting of four steps procedure was selected, two steps for grinding and two steps for polishing. The procedure is described in the machine as follow:
    - 1 Piano (220 µm) (2 minutes)
    - Allegro (3 minutes)
    - DAC (3 µm) (diamond polishing) (3 minutes)
    - Chem OP-AA (oxide polishing) (2 minutes)
- After each of the steps mentioned before, the specimens were thoroughly cleaned on a Struers Lavamin machine (ultrasonic cleaner) to remove any residues from the ground surface.

3.4. Tensile test

The tensile test was performed to study the mechanical properties under uniaxial load. Nine ASTM E8/E8M subsize tensile specimens were used for the experiment. These samples were tested at room temperature in their as-sintered condition. To measure the width and thickness of the samples, a caliper was used. Monotonic tension tests were carried out with an Instron 5895 tensile machine. This machine has the capability of measuring the deformation and the applied load at a given interval. The strain rate control method was used, ASTM control method B. Strain rate was set at 0.015 mm/mm/min for the elastic region and 0.1 mm/mm/min for the plastic region. All tensile tests have been conducted up to a point of fracture or failure. Yield tensile strength (YTS), ultimate tensile strength (UTS), Young's modulus (E) and Elongation (%) were obtained in uniaxial tensile stress condition.

3.5. Optical Light Microscopy (OLM) evaluation

An optical light microscope of type Olympus GX-53 was used to study the macrostructure of 17-4 PH stainless steel. After the grinding and polishing of the specimens, images were taken for analysis. Magnification setting of 2.5x1, 5x1, 10x1, 20x1 50x1 were used. Software OLYMPUS Stream Essential was used to process the images.

4. RESULTS

The results from the tensile test and light microscope evaluation performed with the as-sintered AM 17-4 PH stainless steel samples produced by the BMD technology are shown in this chapter. The tensile tests were performed according to ASTM E8/E8M.

4.1. Tensile test results

All tensile tests specimens were tensioned until fracture. The fracture for specimens XY-flat 1, XY-flat 2, XY-flat 3, ZX 7, ZX 8, and ZX 9 was within the gauge length section, while the fracture for all the XY-sided specimens was outside the gauge length section. The fracture outside the gauge length for the XY-sided specimens could mean a weak area on the region of the fracture caused by the support structure needed during the printing process or a defect caused by the pattern followed by the machine during the printing process. Figure 20 shows all the specimens after fracture.

Figure 20: fracture location of all tensile specimens.

Tensile test results for all 17-4 PH stainless steel as-sintered specimens produced by the BMD process are shown in Table 9. A specimen name Markforged represents the values provided by the manufacturer (see Table 8 on page 40). The results indicate that building orientation has significant effects on the monotonic tensile behavior of 17-4 PH SS. Ultimate tensile strengths and elongation to failure were greatly influenced by part building orientation.

Table 9: Tensile test results for all specimens (Markforged as-sintered represents reference values).

SPECIMEN	0 2% Yield Strength (MPa)	Ultimate Tensile Strength (MPa)	Modulus (Young's) (GPa)	Elongation at Break (%)
Markforged as-sintered	800	1050	140	5
XY-flat 1	661	1072	136,74154	5,2359
XY-flat 2	764,3	1065	115,59285	4,84687
XY-flat 3	638,8	1067	161,52741	4,84015
XY-sided 4	699,8	780,8	135,54382	0,80738
XY-sided 5	637,6	817,5	145,63077	0,95579
XY-sided 6	613,3	846,7	286,87218	0,80171
ZX 7	579,4	737,7	139,73493	1,08553
ZX 8	656,6	725,5	128,67751	0,90921
ZX 9	610,1	717,2	123,82649	0,95042

Tensile test values are shown in the diagrams below. Figure 21 shows the yield strength for all the test specimens and for the reference value. As compared to the reference value with a yield strength of 800 Mpa, all the test specimens (in all orientations) exhibit significant lower yield strength. No explanation to this behavior is given since the comparison is being made with the values presented by the manufacturer of the BMD technology and the values for all the specimens were similar independent of the building orientation. Further testing is required.

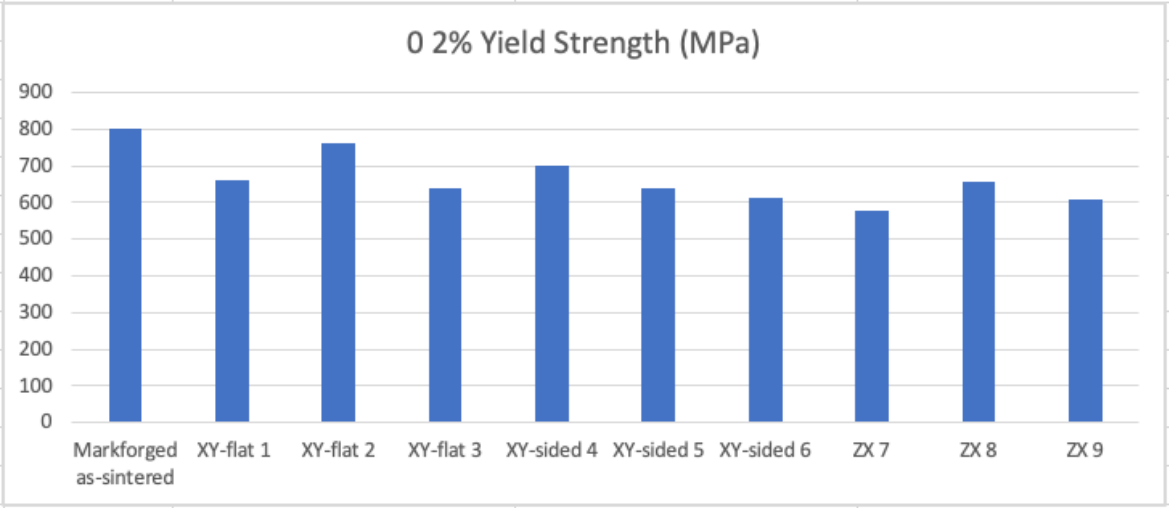

Figure 21: Yield strength for all the test specimen and for the reference value.

Figure 22 shows the ultimate tensile strength for all the test specimens and for the reference value. As compared to the reference value with an ultimate tensile strength of 1050 Mpa, XY-flat specimens (horizontal specimens without support structure during manufacturing) exhibited similar ultimate tensile strength values. This was not the case for all the other specimens where the ultimate tensile strength values are significantly lower compared to the reference value. This can be justified by deposited layer orientation with respect to the axis of tensile loading and manufacturing defects caused by the part orientation. Figure 23 shows the Young´s modulus for all the test specimens and for the reference value. The Modulus of elasticity values for all the test specimens was above or below 20 Mpa around the reference value except for specimen XY-sided 6 which has a remarkable increase, this is thought to be measurement errors, however more samples should be tested to provide a valid conclusion.

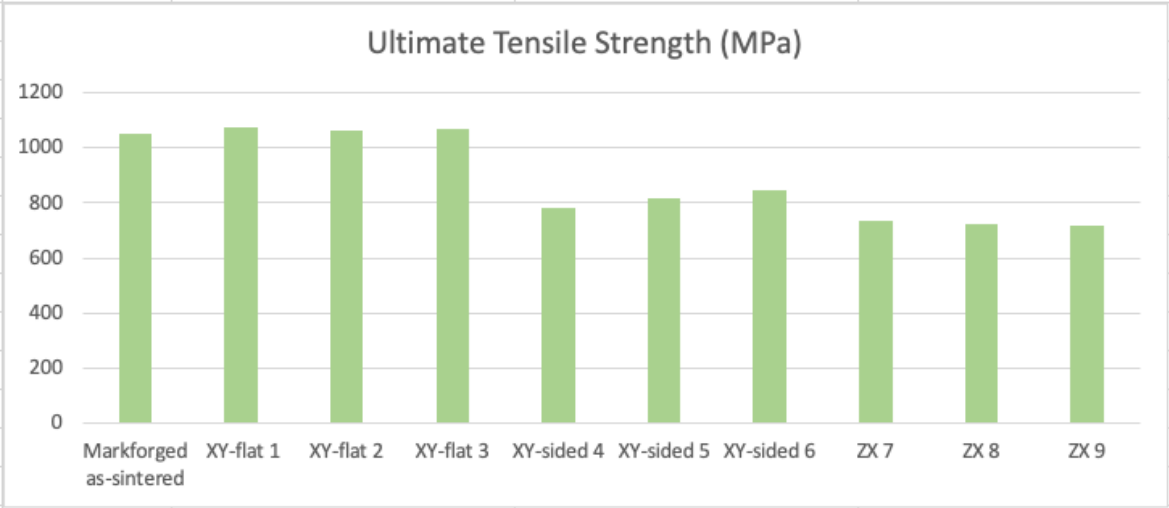

Figure 22: Ultimate tensile strength for all the test specimen and for the reference value.

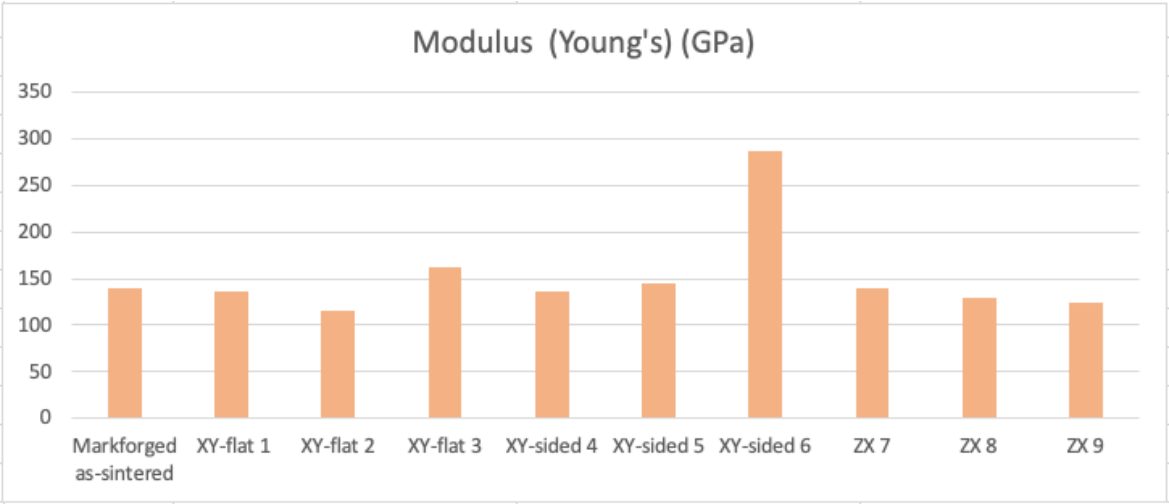

Figure 23: Young´s modulus for all the test specimen and for the reference value.

Figure 24 shows the elongation at break for all the test specimens and for the reference value. Elongation at break of ZX specimens (vertical specimens) and XY-flat specimens (horizontal specimens with support structure during manufacturing) is noticeably lower than that of XY-flat specimens (horizontal specimens without support structure during manufacturing). This can be justified by deposited layer orientation with respect to the axis of tensile loading and manufacturing defects caused by the part orientation. For the vertical specimens the layers are perpendicular to the tensile load direction, providing easier path for void growth and coalescence. For the horizontal specimens the layers are parallel to the loading axis, retarding the opening and expansion of voids. Specimens XY-sided and ZX presented brittle fracture.

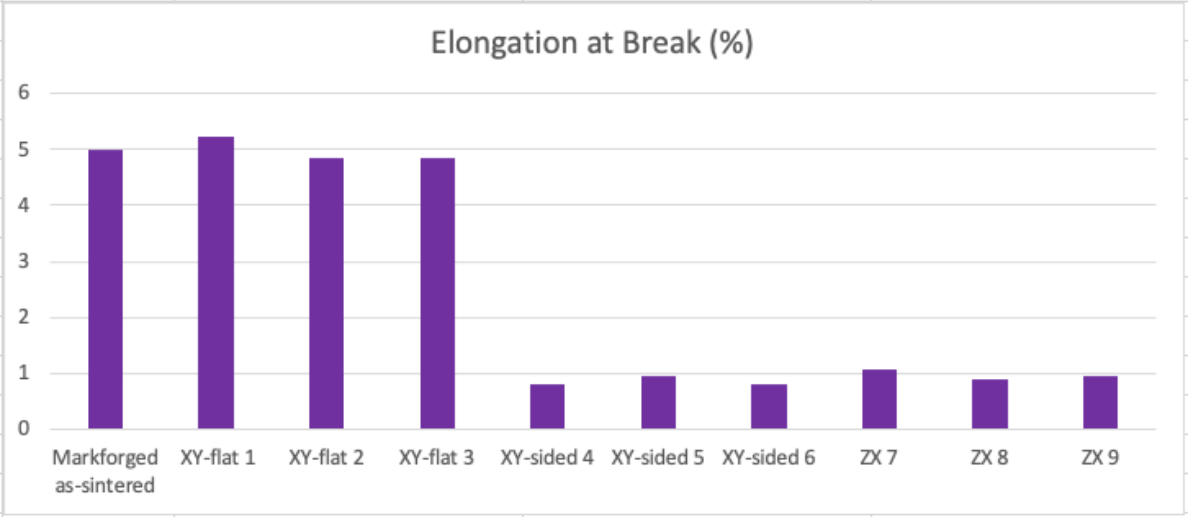

Figure 24: Elongation at break for all the test specimen and for the reference value.

Stress-Strain curves of all the specimens are presented in Figure 25. The stress-strain curve for the three horizontal XY-flat specimens followed the same pattern. The three XY-flat specimens showed very similar ultimate tensile strength and % elongation values. However, the three XY-flat specimens showed different yield strength and E-modulus values. The E-modulus values difference was of about 45 GPa between the maximum and the minimum value. The yield strength difference was of about 125 MPa between the maximum and the minimum value. It was clearly noted that the horizontal XY-flat specimens showed the highest performance since they have the best ductility (elongation at break) and the highest ultimate tensile strength in comparison with all the test specimens.

The three specimens on the horizontal XY-sided direction fractured in the same region outside the gauge length which could mean a weak area on that region because of the support structure

needed during the printing process or a weak area on that region product of the part orientation. The three specimens built in the ZX direction exhibited a high susceptibility to fracture. It can be seen in the strain-stress curve that the strain at break in the specimens built in vertical ZX direction is lower than the strain at break in the specimens built in the horizontal XY-flat direction.

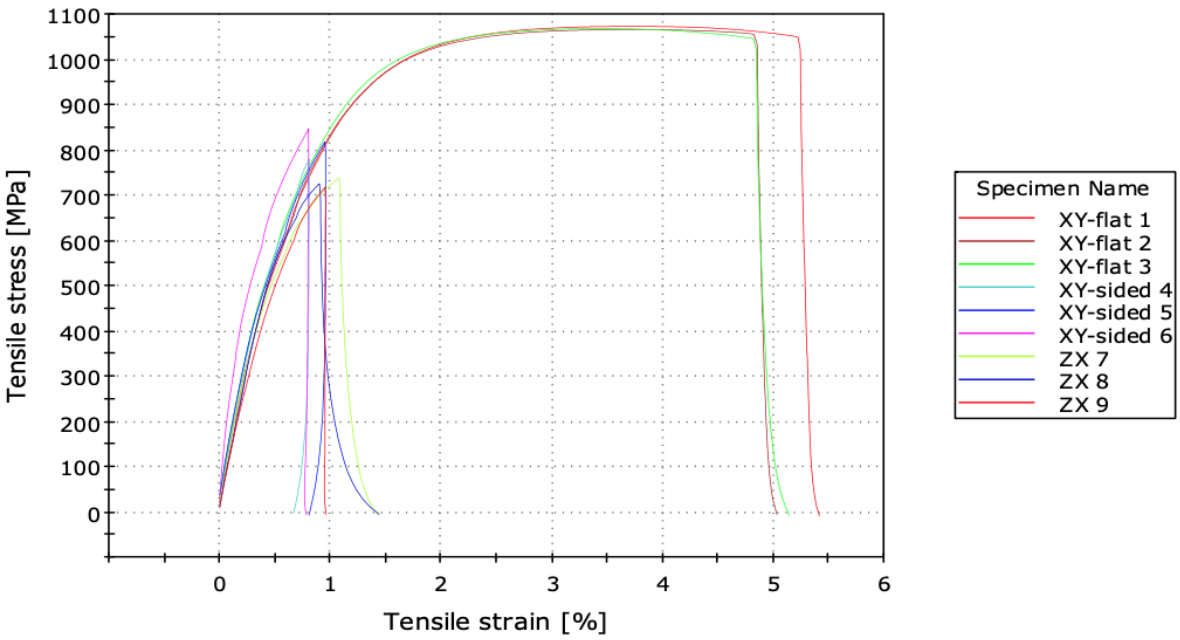

Figure 25*: Engineering stress-strain curve of AM 17-4 PH stainless steel in different building orientations.*

The ultimate tensile stress and % elongation values determined in this work by horizontal specimens XY-flat-1, XY-flat-2 and XY-flat-3 are comparable to the values listed by Markforged for the same type of specimen (as-sintered BMD 17-4 PH stainless steel), but the yield strength values are lower. Elongation to failure was noticeably influenced by specimen building orientation. It is clearly noticed that vertical ZX specimens have lower elongation to failure values than horizontally XY-flat specimens. Generally, the yield strength values obtained in this experiment are low in comparison to the values presented by Markforged. The results indicate that building orientation with respect to the axis of tensile loading have significant effect on the monotonic tensile behavior of AM 17-4 PH stainless steel as sintered.

4.2. Optical Light Microscope results

The images taken from the optical light microscope are shown in the following figures below (Figure 26, Figure 27, Figure 28, and Figure 29). Figure 26 and Figure 28 show the cross section of the specimens parallel to the direction of the printing layer orientation (top view). Figure 27 and Figure 29 show the cross section of the specimens perpendicular to the direction of the printing layer orientation (side view).

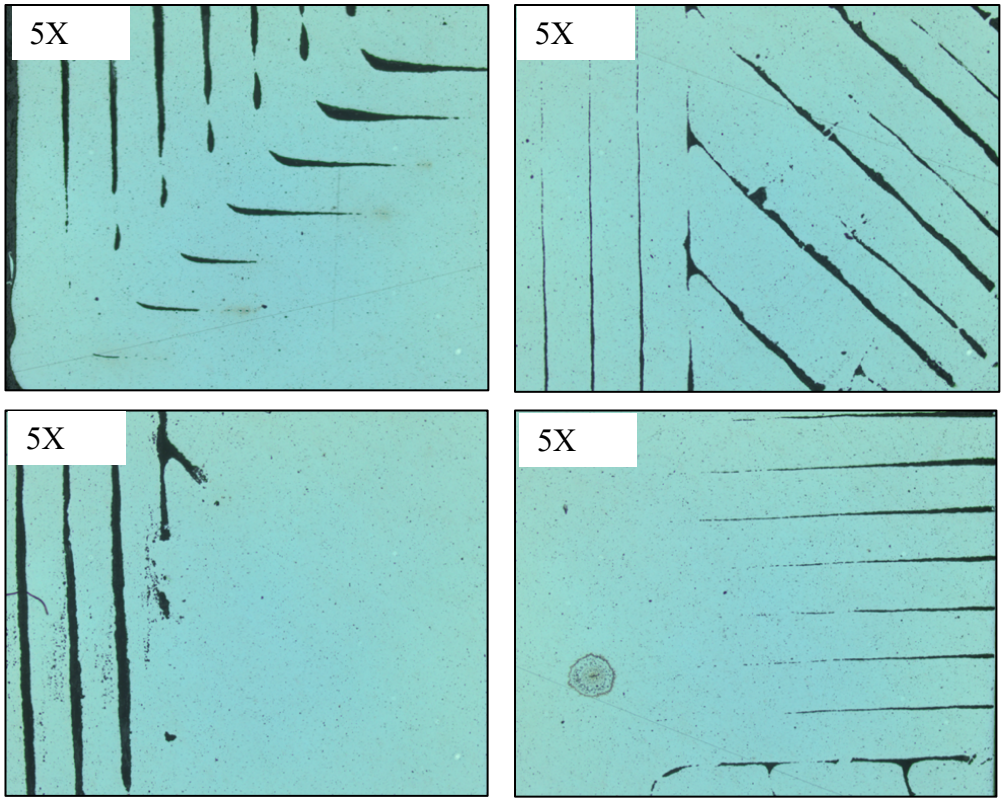

Figure 26: Top view of vertically printed specimens

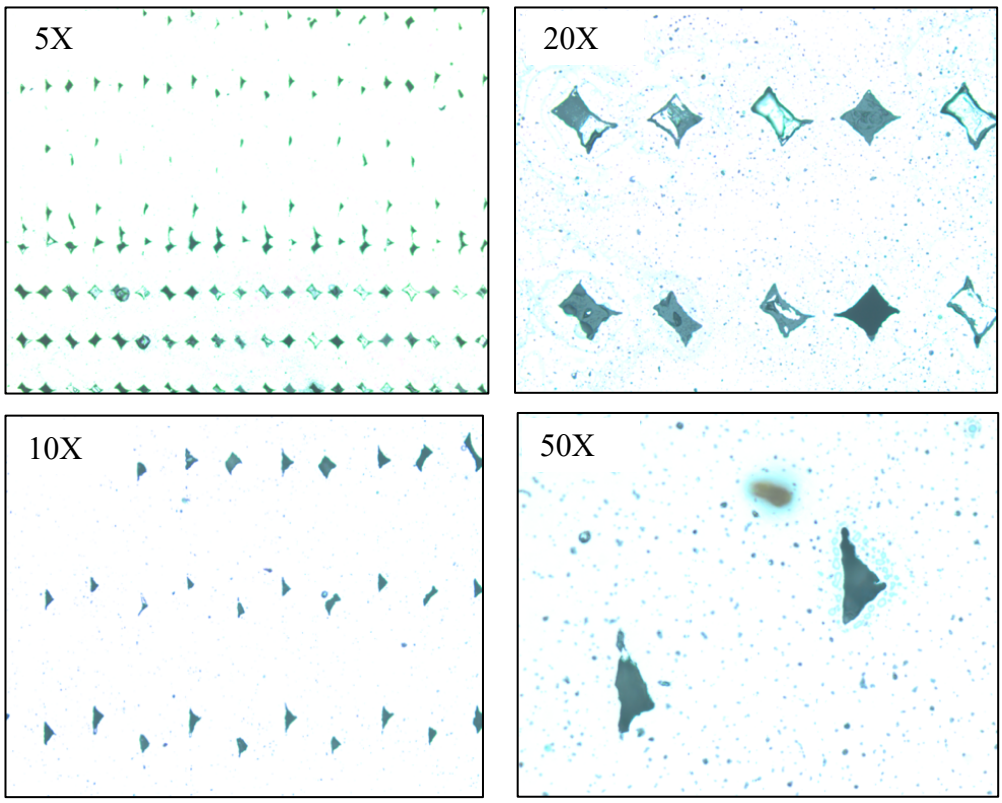

Figure 27: Side view of vertically printed specimens.

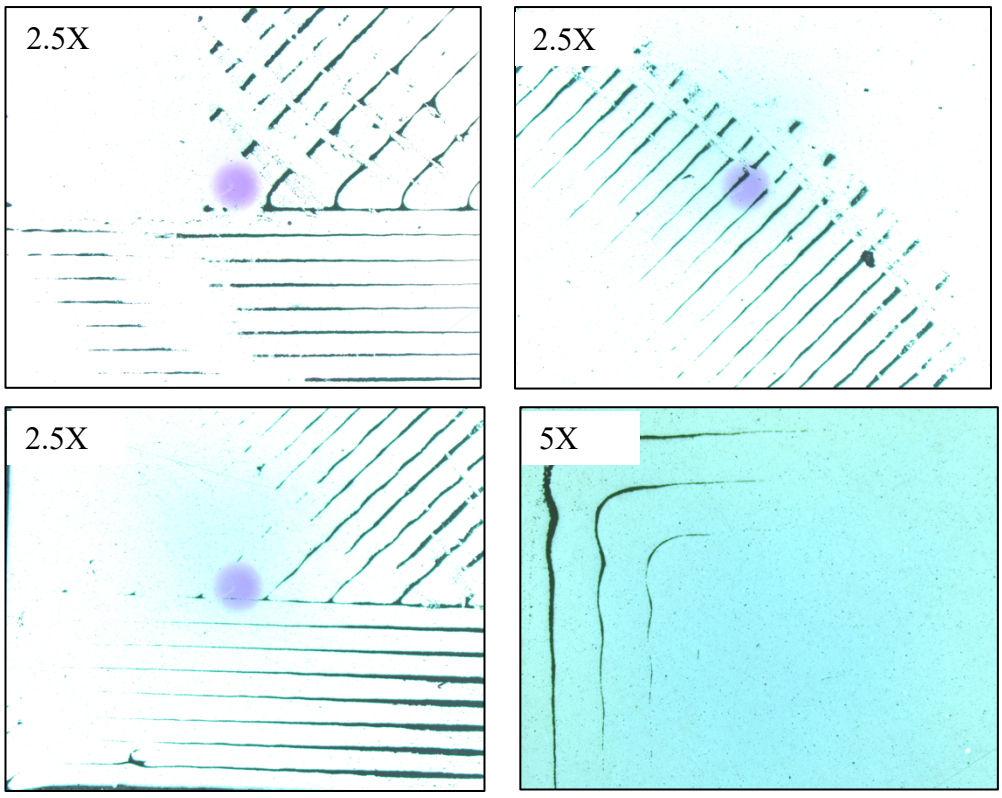

Figure 28: Top view of horizontally printed specimens.

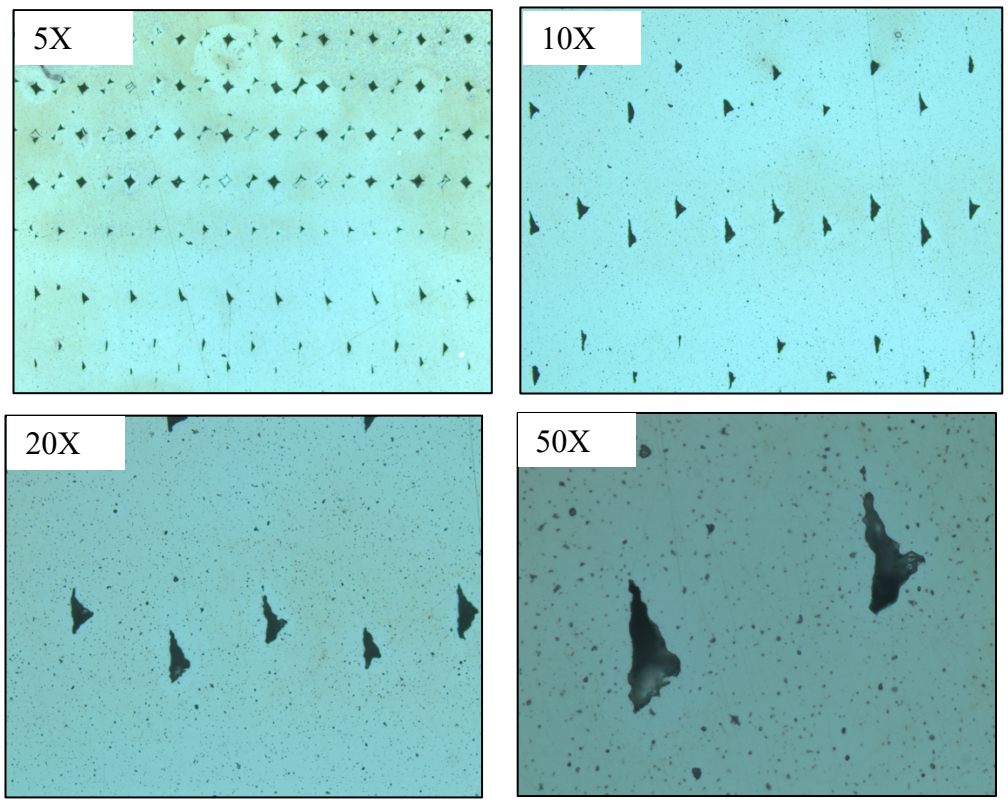

Figure 29: Side view of horizontally printed specimens

From the images taken from the optical light microscope, the printing pattern was easy to identify. This pattern is clearly shown from the top view of both specimens, the vertically printed (Figure 26), and the horizontally printed (Figure 28). Printed layers can be seen to be of more or less constant dimensions. The images also revealed un-melted regions between layers. These un-melted regions of irregular shape, called voids, covered a large cross-sectional region. The systematic pattern of these unmelted regions reduces the cross-sectional area and can have a large effect on the strength of the printed part. These defects can also act as stress concentration sites when oriented perpendicular to the build direction. From the side view of both specimens, the vertically printed (Figure 27), and the horizontally printed (Figure 29), it can be seen that close to the edges these voids are diamond shaped and away from the edges are triangular shaped. This difference in shape can be related to the pattern followed by the printer machine, since it starts with a perimeter raster and then a ± 45° solid infill alternating between layers. The area of the triangular shaped voids was of about 750 μm^2 and the area of the diamond shaped voids was of about 2100 μm^2. Many spherical pores were also observed across the section.

5. DISCUSSION

5.1. Literature review:

This review investigates the available information to the present time on additive manufacturing of metals and fatigue performance of additive manufacture parts but does not cover all the work published in the area. AM of metals is a process that fabricates metal parts starting from a 3D model in a computer and then the model is sent to the AM machine to produce the part layer by layer. There are many AM technologies commercially available. These can be generally classified as powder bed system, powder fed system and wire fed system.

The fabrication processes of AM metal parts involve many parameters that affect the final product. An improper selection of these process parameters can lead to internal defects and surface defects. Fabrication induced internal defects, and surface defects unavoidable in the layer-by-layer AM processes can serve as crack initiation sites and affect the fatigue performance of AM produced alloys. Internal defects such as porosity are related to the initial powder condition and process parameters and are generally spherical in shape. Internal defects such as voids are caused by incomplete bonding between successive layers. Voids are irregular in shape and are generally larger than porosity defects. Voids defects are found to have more detrimental effect on fatigue performance than porosity defects due to the larger size and irregular shape. HIP (hot isostatic pressing) treatment has a significant effect if the AM part goes through machine treatment as well, because surface defects control the cracking behavior of the AM part, even after healing the internal defects with HIP treatment.

The building orientation of the metal AM parts also influences its fatigue behavior. Specimens printed with the layer planes parallel to the load axis of the specimen (horizontal specimen) present longer fatigue lives than specimens printed with the layer planes perpendicular to the load axis of the specimens (vertical specimen). This is because for vertical printed specimens the major axis of an un-melted region is perpendicular to the loading axis, providing much higher stress concentration, and therefore, lower crack initiation resistance.

5.2. Tensile test:

The specimens fabricated in the horizontal direction without any support, XY-flat specimens, presented ultimate tensile stress and % elongation values, comparable to the values listed by Markforged for the same type of specimen (as-sintered BMD 17-4 PH stainless steel), but the yield strength values were lower.

The specimens fabricated in the vertical direction, ZX specimens, presented lower UTS, yield strength, and % elongation values compared to the values listed by Markforged for the same type of specimen (as-sintered BMD 17-4 PH stainless steel).

The specimens fabricated in the horizontal direction with support, XY-sided specimens, presented lower UTS, yield strength, and % elongation values compared to the values listed by Markforged for the same type of specimen (as-sintered BMD 17-4 PH stainless steel) and fractured outside the gauge length.

The results obtained with the tensile test show that the building orientation of the specimens affects the mechanical properties of the metal parts. It can be seen that the directionality of defects such as voids can influence the anisotropy in mechanical properties. For vertically built specimens, tensile stresses are perpendicular to the plane of the defects. This leads to crack propagation along the tip of the defect, resulting in material failure. This corresponds with earlier research of the mechanical properties of metal additive manufactured parts (Alsalla et al., 2018; Kok et al., 2018; Shamsaei et al., 2015). Also, the reduction of the mechanical properties may have been due to the lack of machining of the exterior surfaces.

6. CONCLUSION

Fatigue performance of metal AM parts has been found to be influenced by the fabrication defects characteristic to the metal AM process. These defects include internal and surface defects such as residual stresses, rough surface and microstructural inhomogeneities. Voids (inter-layer cavities from unmelted regions) are found to be more detrimental than pores (spherical shaped resulting from entrapped gas) due to the larger size and irregular shape. Their larger size and irregular shape create higher stress concentration than spherical shaped pores.

The process parameters that most influence the fatigue performance are heat input, building direction, surface finish and heat treatment. Heat treatments include stress relieving, annealing and HIP. Surface treatments include machining, polishing or peening.

Post fabrication process operations such as machining to reduce or eliminate the surface defects improve the fatigue life of metal AM parts in general. Machining minimizes the surface roughness and imperfections close to the surface and therefore reduces the stress concentration. HIP processes homogenize the microstructure and reduce the porosity by closing the internal pores. However, post fabrication processes such as heat treatment without surface finish operations do not always improve the fatigue life of metal AM parts because the main contributors in controlling the cracking behavior are the stress concentration effects of surface roughness.

The building orientation has also influence on the fatigue behavior. Vertically manufactured specimens show lower fatigue strength than horizontally manufactured specimens. This is mainly attributed to the orientation of the deposited layers with respect to the applied loading direction. For vertically printed specimens the larger area of an un-melted region is perpendicular to the loading axis, therefore the stress concentration of the un-melted region is higher and more susceptible to opening and initiating crack.

The tensile test performed during this investigation on the as-sintered AM 17-4 PH stainless steel fabricated by the BMD method showed that the building orientation affects the mechanical properties of the material under monotonic loading (tensile behavior). The weaker build strategy recorded was in the XY-sided direction where the specimens needed support during the building process. A weak zone in the part could have been the result of the pattern followed by the printer machine, or the support structure could have created a weak zone in the

part. Vertically built specimens (ZX specimens) showed lower elongation to failure than the horizontally built specimens (XY-flat specimens). This could have been because on vertically built specimens, defects formed between layers are perpendicular to the tensile load direction. This provides an easy path for void growth and coalescence under tensile loading, resulting in lower strength when loaded in this direction. In terms of ductility and tensile strength, the horizontally built specimens without any support, XY-flat specimens, proved to be the strongest build direction. Further studies on the BMD method are required to find more precise tensile and yield values among the different building orientations.

Due to the significant diversity of AM technologies and the fact that the fatigue behavior of AM parts is dependent on manufacturing conditions, building orientation, internal defects and other parameters, the standardization of the processes is needed. Even though standards for additive manufacturing methods, tests, and terminology exist, these do not appear to be widely used in existing research. One reason could be that these standards are evolving with the technology. Organizations such as DNV, ISO and ASTM are working on standardization or already have some standards. In general, further study is still required to better understand the final properties of AM parts and to better evaluate and predict their optimal fatigue design.

7. REFERENCES

Afkhami, S., Dabiri, M., Alavi, S. H., Björk, T., & Salminen, A. (2019). Fatigue characteristics of steels manufactured by selective laser melting. *International Journal of Fatigue, 122*, 72-83. doi:10.1016/j.ijfatigue.2018.12.029

AK Steel. 17-4 PH Stainless Steel. Retrieved from https://www.aksteel.com

Alsalla, H. H., Smith, C., & Hao, L. (2018). Effect of build orientation on the surface quality, microstructure and mechanical properties of selective laser melting 316L stainless steel. *Rapid Prototyping Journal, 24*(1), 9-17. doi:10.1108/rpj-04-2016-0068

ASTM International. (2021a). Additive Manufacturing Overview. Retrieved from https://www.astm.org/industry/additive-manufacturing-overview.html

ASTM international. (2021b). *ASTM E8 / E8M-21*. Retrieved from West Conshohocken, PA: https://www.astm.org

Blinn, B., Klein, M., Gläßner, C., Smaga, M., Aurich, J. C., & Beck, T. (2018). An Investigation of the Microstructure and Fatigue Behavior of Additively Manufactured AISI 316L Stainless Steel with Regard to the Influence of Heat Treatment. *Metals, 8*(4), 220. Retrieved from https://www.mdpi.com/2075-4701/8/4/220

Brandt, M. (2016). *Laser Additive Manufacturing : Materials, Design, Technologies, and Applications*. Cambridge, UNITED KINGDOM: Elsevier Science & Technology.

Carneiro, L., Jalalahmadi, B., Ashtekar, A., & Jiang, Y. (2019). Cyclic deformation and fatigue behavior of additively manufactured 17–4 PH stainless steel. *International Journal of Fatigue, 123*, 22-30. doi:https://doi.org/10.1016/j.ijfatigue.2019.02.006

Chern, A. H., Nandwana, P., Yuan, T., Kirka, M. M., Dehoff, R. R., Liaw, P. K., & Duty, C. E. (2019). A review on the fatigue behavior of Ti-6Al-4V fabricated by electron beam melting additive manufacturing. *International Journal of Fatigue, 119*, 173-184. doi:https://doi.org/10.1016/j.ijfatigue.2018.09.022

Dass, A., & Moridi, A. (2019). State of the Art in Direct Energy Deposition: From Additive Manufacturing to Materials design. *Coatings 9*(7), 418. doi:10.3390/coatings9070418

Davis, J. R. (2004). *Tensile Testing* (2 ed.). Materials Park, UNITED STATES: A S M International.

DebRoy, T., Wei, H. L., Zuback, J. S., Mukherjee, T., Elmer, J. W., Milewski, J. O., . . . Zhang, W. (2018). Additive manufacturing of metallic components – Process, structure and properties. *Progress in Materials Science, 92*, 112-224. doi:10.1016/j.pmatsci.2017.10.001

Desktop Metal. (2021). Deep Dive: Bound Metal Deposition (BMD). Retrieved from https://www.desktopmetal.com/resources/deep-dive-bmd

Dutta, B., Babu, S., & Jared, B. H. (2019). *Science, Technology and Applications of Metals in Additive Manufacturing*. San Diego, UNITED STATES: Elsevier.

Elangeswaran, C., Cutolo, A., Muralidharan, G. K., de Formanoir, C., Berto, F., Vanmeensel, K., & Van Hooreweder, B. (2019). Effect of post-treatments on the fatigue behaviour of 316L stainless steel manufactured by laser powder bed fusion. *International Journal of Fatigue, 123*, 31-39. doi:10.1016/j.ijfatigue.2019.01.013

Fatemi, A., Molaei, R., & Phan, N. (2020). Multiaxial fatigue of additive manufactured metals: Performance, analysis, and applications. *International Journal of Fatigue, 134*. doi:10.1016/j.ijfatigue.2020.105479

Fatemi, A., Molaei, R., Sharifimehr, S., Shamsaei, N., & Phan, N. (2017). Torsional fatigue behavior of wrought and additive manufactured Ti-6Al-4V by powder bed fusion including surface finish effect. *International Journal of Fatigue, 99*, 187-201. doi:https://doi.org/10.1016/j.ijfatigue.2017.03.002

Fatemi, A., Molaei, R., Simsiriwong, J., Sanaei, N., Pegues, J., Torries, B., . . . Shamsaei, N. (2019). Fatigue behaviour of additive manufactured materials: An overview of some recent experimental studies on Ti-6Al-4V considering various processing and loading direction effects. *Fatigue & fracture of engineering materials & structures, 42*(5), 991-1009. doi:10.1111/ffe.13000

Frazier, W. E. (2014). Metal Additive Manufacturing: A Review. *Journal of Materials Engineering and Performance, 23*(6), 1917-1928. doi:10.1007/s11665-014-0958-z

Gibson, I., Rosen, D., & Stucker, B. (2015). *Additive Manufacturing Technologies: 3D Printing, Rapid Prototyping, and Direct Digital Manufacturing* (2 ed.). New York, NY: Springer

Halada, G. P., & Clayton, C. R. (2018). The Intersection of Design, Manufacturing, and Surface Engineering. In M. Kutz (Ed.), *Handbook of Environmental Degradation of Materials* (3 ed., pp. 397-422): William Andrew Publishing.

Herzog, D., Seyda, V., Wycisk, E., & Emmelmann, C. (2016). Additive manufacturing of metals. *Acta Materialia, 117*, 371-392. doi:10.1016/j.actamat.2016.07.019

Holgate, J. H., & Webb, J. (2003). MICROSCOPY | Light Microscopy and Histochemical Methods. In B. Caballero (Ed.), *Encyclopedia of Food Sciences and Nutrition (Second Edition)* (pp. 3917-3922). Oxford: Academic Press.

Johnson, A. S., Shao, S., Shamsaei, N., Thompson, S. M., & Bian, L. (2017). Microstructure, Fatigue Behavior, and Failure Mechanisms of Direct Laser-Deposited Inconel 718. *JOM, 69*(3), 597-603. doi:10.1007/s11837-016-2225-2

Kok, Y., Tan, X. P., Wang, P., Nai, M. L. S., Loh, N. H., Liu, E., & Tor, S. B. (2018). Anisotropy and heterogeneity of microstructure and mechanical properties in metal additive manufacturing: A critical review. *Materials & Design, 139*, 565-586. doi:https://doi.org/10.1016/j.matdes.2017.11.021

Li, C., Liu, Z. Y., Fang, X. Y., & Guo, Y. B. (2018). Residual Stress in Metal Additive Manufacturing. *Procedia CIRP, 71*, 348-353. doi:https://doi.org/10.1016/j.procir.2018.05.039

Li, P., Warner, D. H., Fatemi, A., & Phan, N. (2016). Critical assessment of the fatigue performance of additively manufactured Ti–6Al–4V and perspective for future research. *International Journal of Fatigue, 85*, 130-143. doi:https://doi.org/10.1016/j.ijfatigue.2015.12.003

Liverani, E., Toschi, S., Ceschini, L., & Fortunato, A. (2017). Effect of selective laser melting (SLM) process parameters on microstructure and mechanical properties of 316L austenitic stainless steel. *Journal of Materials Processing Technology, 249*, 255-263. doi:https://doi.org/10.1016/j.jmatprotec.2017.05.042

Markforged. (2021). Material Datasheet: 17-4 PH Stainless Steel. Retrieved from https://static.markforged.com/downloads/17-4-ph-stainless-steel.pdf

Milewski, J. O. (2017). *Additive Manufacturing of metals* (Vol. 258). Cham: Springer Nature.

Miroslav, P., Pavlĺna, T., Jana, H., Pavel, Š., & Boiviek, K. (2017). A Study of Selective Laser Melting Technology on the Ultra-High Strength Tool Steel Use—Quality, Mechanical Properties and Fatigue. In *Boukharouba T., Pluvinage G., Azouaoui K. (eds) Applied Mechanics, Behavior of Materials, and Engineering Systems. Lecture notes in Mechanical Engineering.* (pp. 67-86): Springer, Cham.

Mirzadeh, H., & Najafizadeh, A. (2009). Aging kinetics of 17-4 PH stainless steel. *Materials Chemistry and Physics, 116*(1), 119-124. doi:https://doi.org/10.1016/j.matchemphys.2009.02.049

Molaei, R., & Fatemi, A. (2019). Crack paths in additive manufactured metallic materials subjected to multiaxial cyclic loads including surface roughness, HIP, and notch effects. *International Journal of Fatigue, 124*, 558-570. doi:10.1016/j.ijfatigue.2019.03.007

Molaei, R., Fatemi, A., Sanaei, N., Pegues, J., Shamsaei, N., Shao, S., . . . Phan, N. (2020). Fatigue of additive manufactured Ti-6Al-4V, Part II: The relationship between

microstructure, material cyclic properties, and component performance. *International Journal of Fatigue, 132*. doi:10.1016/j.ijfatigue.2019.105363

Nezhadfar, P. D., Burford, E., Anderson-Wedge, K., Zhang, B., Shao, S., Daniewicz, S. R., & Shamsaei, N. (2019). Fatigue crack growth behavior of additively manufactured 17-4 PH stainless steel: Effects of build orientation and microstructure. *International Journal of Fatigue, 123*, 168-179. doi:10.1016/j.ijfatigue.2019.02.015

Ngo, T. D., Kashani, A., Imbalzano, G., Nguyen, K. T. Q., & Hui, D. (2018). Additive manufacturing (3D printing): A review of materials, methods, applications and challenges. *Composites Part B: Engineering, 143*, 172-196. doi:10.1016/j.compositesb.2018.02.012

Pegues, J. W., Shao, S., Shamsaei, N., Sanaei, N., Fatemi, A., Warner, D. H., . . . Phan, N. (2020). Fatigue of additive manufactured Ti-6Al-4V, Part I: The effects of powder feedstock, manufacturing, and post-process conditions on the resulting microstructure and defects. *International Journal of Fatigue, 132*. doi:10.1016/j.ijfatigue.2019.105358

Poulin, J. R., Kreitcberg, A., Terriault, P., & Brailovski, V. (2020). Fatigue strength prediction of laser powder bed fusion processed Inconel 625 specimens with intentionally-seeded porosity: Feasibility study. *International Journal of Fatigue, 132*. doi:10.1016/j.ijfatigue.2019.105394

Prabhu, A. W., Vincent, T., Chaudhary, A., Zhang, W., & Babu, S. S. (2015). Effect of microstructure and defects on fatigue behaviour of directed energy deposited Ti–6Al–4V. *Science and Technology of Welding and Joining, 20*(8), 659-669. doi:10.1179/1362171815Y.0000000050

Shamsaei, N., Yadollahi, A., Bian, L., & Thompson, S. M. (2015). An overview of Direct Laser Deposition for additive manufacturing; Part II: Mechanical behavior, process parameter optimization and control. *Additive Manufacturing, 8*, 12-35. doi:10.1016/j.addma.2015.07.002

Spierings, A. B., Starr, T. L., & Wegener, K. (2013). Fatigue performance of additive manufactured metallic parts. *Rapid Prototyping Journal, 19*(2), 88-94. doi:10.1108/13552541311302932

Tang, M., & Pistorius, P. C. (2019). Fatigue life prediction for AlSi10Mg components produced by selective laser melting. *International Journal of Fatigue, 125*, 479-490. doi:10.1016/j.ijfatigue.2019.04.015

Wang, Z., Wu, W., Qian, G., Sun, L., Li, X., & Correia, J. A. F. O. (2019). In-situ SEM investigation on fatigue behaviors of additive manufactured Al-Si10-Mg alloy at

elevated temperature. *Engineering Fracture Mechanics, 214*, 149-163. doi:10.1016/j.engfracmech.2019.03.040

Yadollahi, A., Shamsaei, N., Thompson, S. M., Elwany, A., & Bian, L. (2017). Effects of building orientation and heat treatment on fatigue behavior of selective laser melted 17-4 PH stainless steel. *International Journal of Fatigue, 94*, 218-235. doi:https://doi-org.ezproxy.uis.no/10.1016/j.ijfatigue.2016.03.014

Yang, K. V., Rometsch, P., Jarvis, T., Rao, J., Cao, S., Davies, C., & Wu, X. (2018). Porosity formation mechanisms and fatigue response in Al-Si-Mg alloys made by selective laser melting. *Materials Science and Engineering: A, 712*, 166-174. doi:https://doi.org/10.1016/j.msea.2017.11.078

Yuan, L. (2019). Solidification Defects in Additive Manufactured Materials. *JOM, 71*(9), 3221-3222. doi:10.1007/s11837-019-03662-x

Zadi-Maad, A., Rohib, R., & Irawan, A. (2018). *Additive manufacturing for steels: a review*. Paper presented at the Mineral Processing and Technology International Conference 2017.

Zhai, Y., Galarraga, H., & Lados, D. A. (2016). Microstructure, static properties, and fatigue crack growth mechanisms in Ti-6Al-4V fabricated by additive manufacturing: LENS and EBM. *Engineering Failure Analysis, 69*, 3-14. doi:https://doi.org/10.1016/j.engfailanal.2016.05.036

FIGURES

Figure 1: PBF-L system. Reprinted from Progress in Materials Science, 92, T. DebRoy, H. L. Wei, J. S. Zuback, T. Mukherjee, J. W. Elmer, J. O. Milewski, A. M. Beese, A. Wilson-Heid, A. De, W. Zhang, Additive manufacturing of metallic components – Process, structure and properties, 112-224, Copyright (2018), with permission from Elsevier.

Figure 2: PBF-EB system. Reprinted by permission from Springer Nature: Springer Nature, Additive Manufacturing Technologies: 3D Printing, Rapid Prototyping, and Direct Digital Manufacturing by Ian Gibson, David Rosen, Brent Stucker, Copyright (2015).

Figure 3: DED-L system with metal powder used as feedstock material. Reprinted from Progress in Materials Science, 92, T. DebRoy, H. L. Wei, J. S. Zuback, T. Mukherjee, J. W. Elmer, J. O. Milewski, A. M. Beese, A. Wilson-Heid, A. De, W. Zhang, Additive manufacturing of metallic components – Process, structure and properties, 112-224, Copyright (2018), with permission from Elsevier.

Figure 4: DED-EB system with metal wire used as feedstock material. Reprinted from Progress in Materials Science, 92, T. DebRoy, H. L. Wei, J. S. Zuback, T. Mukherjee, J. W. Elmer, J. O. Milewski, A. M. Beese, A. Wilson-Heid, A. De, W. Zhang, Additive manufacturing of metallic components – Process, structure and properties, 112-224, Copyright (2018), with permission from Elsevier.

Figure 5: DED-PA system with metal wire used as feedstock material. Reprinted from Progress in Materials Science, 92, T. DebRoy, H. L. Wei, J. S. Zuback, T. Mukherjee, J. W. Elmer, J. O. Milewski, A. M. Beese, A. Wilson-Heid, A. De, W. Zhang, Additive manufacturing of metallic components – Process, structure and properties, 112-224, Copyright (2018), with permission from Elsevier.

Figure 6: BMD 3D Printer. Own creation.

Figure 7: BMD Debinder. Own creation.

Figure 8: BMD Furnace. Own creation.

Figure 9: Defects in PBF-L Ti-6Al-4V alloy (A) porosity (entrapped gas) and lack of fusion voids, (B) cracking from a porosity (entrapped gas), (C) lack of fusion voids, (D) crack

initiation and growth from lack of fusion voids defects. Reprinted by permission from John Wiley and Sons, Fatigue behaviour of additive manufactured materials: An overview of some recent experimental studies on Ti-6Al-4V considering various processing and loading direction effects by A. Fatemi, R. Molaei, J. Simsiriwong, et al, © 2019 Wiley Publishing Ltd.

Figure 10: Building direction. *Own creation.*

Figure 11: "Reprinted from International Journal of Fatigue, 94 / 2, A. Yadollahi, N. Shamsaei, Scott M. Thompson, A. Elwany, L. Bian. Effects of building orientation and heat treatment on fatigue behavior of selective laser melted 17-4 PH stainless steel, 218-235, Copyright (2017), with permission from Elsevier.

Figure 12: Engineering strain-stress curve. Republished with permission of ASM International, from Tensile Testing, J. R. Davis ,2nd edition, 2004; permission conveyed through Copyright Clearance Center, Inc.

Figure 13: Standard tensile bar with dimension according to ASTM E8/E8M. *Own creation.*

Figure 14: BMD tensile testing sample manufactured at the XY-flat building orientation. *Own creation.*

Figure 15: BMD tensile testing sample manufactured at the XY-sided building orientation. *Own creation.*

Figure 16: BMD tensile testing sample manufactured at the ZX building orientation. *Own creation.*

Figure 17: Illustration of the 2 building directions V and H. *Own creation.*

Figure 18: Raster strategy for an XY-flat subsize tensile specimen. *Own creation*

Figure 19: Specimen mounted in transparent resin. *Own creation.*

Figure 20: fracture location of all tensile specimens. *Own creation.*

Figure 21: Yield strength for all the test specimen and for the reference value. *Own creation.*

Figure 22: Ultimate tensile strength for all the test specimen and for the reference value. *Own creation*

Figure 23: Young´s modulus for all the test specimen and for the reference value. *Own creation.*

Figure 24: Elongation at break for all the test specimen and for the reference value. *Own creation.*

Figure 25: Engineering stress-strain curve of AM 17-4 PH stainless steel in different building orientations. *Own creation.*

Figure 26: Top view of vertically printed specimens. *Own creation*

Figure 27: Side view of vertically printed specimens. *Own creation*

Figure 28: Top view of vertically printed specimens. *Own creation*

Figure 29: Side view of vertically printed specimens. *Own creation*

TABLES

Table 1: Most customary types of metals alloys offered and its applications. Reprinted by permission from Springer Nature: Springer Nature, Additive Manufacturing of Metals: From Fundamental Technology to Rocket Nozzles, Medical Implants, and Custom Jewelry by John O. Milewski, Copyright (2017).

Table 2: AM metal machine manufacturers and their specific process names. Reprinted by permission from Springer Nature: Springer Nature, Additive Manufacturing of Metals: From Fundamental Technology to Rocket Nozzles, Medical Implants, and Custom Jewelry by John O. Milewski, Copyright (2017).

Table 3: Summary of the AM processes. *Own creation.*

Table 4: Critical parameters that control DED and PBF processes. Reprinted from Science, Technology and Applications of Metals in Additive Manufacturing, B. Dutta, S. Babu, B. Jared, Additive manufacturing technology, 11-53, Copyright (2019), with permission from Elsevier.

Table 5: List of SLM steels present in the fatigue studies. Reprinted from International Journal of Fatigue, 122, S. Afkhami, M. Dabiri, S. H. Alavi, T. Björk, & A. Salminen, Fatigue

characteristics of steels manufactured by selective laser melting, 72-83, https://doi.org/10.1016/j.ijfatigue.2018.12.029, under the terms of the http://creativecommons.org/licenses/by-nc-nd/4.0/

Table 6: Failure mechanisms of the PBF-L AM 17-4 PH Stainless Steel, PBF-L AM Ti-6Al-4V and wrought specimens under different conditions. Reprinted from International Journal of Fatigue, 124, R. Molaei, A. Fatemi, Crack paths in additive manufactured metallic materials subjected to multiaxial cyclic loads including surface roughness, HIP, and notch effects, 558-570, Copyright (2019), with permission from Elsevier.

Table 7: Composition of 17-4 PH Stainless Steel (Markforged, 2021).

Table 8: Typical mechanical properties of Markforged 17-4 PH Stainless Steel samples as-sintered fabricated by the BMD method (Markforged, 2021).

Table 9: Tensile test results for all specimens (Markforged as-sintered represents reference values). *Own creation.*